COVER PAGE

This manuscript, <u>Comparing Aggradation, Superelevation, and Avulsion Frequency of Submarine and Fluvial Channels</u>, is a preprint and has been submitted for publication in "Frontiers in Earth Science." The manuscript is currently in peer-review but has not had final acceptance and therefore subsequent versions of this manuscript may have updated content. Please feel free to contact the lead author Zane Jobe ([zanejobe@mines.edu](mailto:zanejobe@mines.edu) or [zanejobe@gmail.com](mailto:zanejobe@gmail.com)) with questions or comments regarding the manuscript.

# Comparing Aggradation, Superelevation, and Avulsion Frequency of Submarine and Fluvial Channels

Zane Jobe[1], Nick Howes[2], Kyle Straub[3], Dingxin Cai[1], Hang Deng[1], Fabien Laugier[4], Luke Pettinga[1], Lauren Shumaker[1]

1. Colorado School of Mines, Golden CO zanejobe@gmail.com or zanejobe@mines.edu
2. Mathworks, Natick MA
3. Tulane University, New Orleans, LA
4. Chevron Energy Technology Company, Houston TX

## Abstract

Constraining the avulsion dynamics of rivers and submarine channels is essential for predicting the distribution and architecture of sediment, organic matter and pollutants in alluvial, deltaic, and submarine settings. Submarine channels are well known to be more aggradational than rivers, and aggradation of the channel, levee, and floodplain are key forcing mechanisms for avulsion. We create a geometric channel-belt framework relating channel, levee, and floodplain stratigraphy that allows comparative analysis of avulsion dynamics for rivers and submarine channels. We utilize 52 channel cross sections within this framework to provide avulsion criteria for submarine channels and how they differ from rivers.

Superelevation and a new channel-floodplain coupling metric are the two key parameters that control channel-belt thickness in both rivers and submarine channels. While rivers can only superelevate an amount equivalent to 1 channel depth above the floodplain prior to avulsion, submarine channels are more stable during aggradation, with superelevation values commonly >3 channel depths. Channel-floodplain coupling in rivers is weak, with floodplain aggradation being negligible compared to channel aggradation. However, floodplain aggradation is more significant for submarine channels, resulting in stronger channel-floodplain coupling.

The combination of enhanced superelevation and strong channel-floodplain coupling results in channel-belts for submarine channels that can be as thick as ~ 10 channel depths, while fluvial channel belts are limited to 2 channel depths. We interpret that levee aggradation and thus superelevation is promoted by

turbidity current overspill. Floodplain aggradation is also influenced by overspill and hemipelagic sedimentation. As a submarine channel reaches aggradation that would cause a river to avulse, the submarine channel is stable because the flow has far less potential energy to create an avulsion because turbidity currents have ~50x less density contrast between flow and ambient fluid as compared to rivers. The Amazon channel showcases this stability, with a channel belt that is ~ 5 channel-depths thick for more than 400 streamwise km, more than twice the aggradation that a river is capable of.

## Introduction

Rivers and submarine channels have similar planform morphologies (Flood and Damuth, 1987; Pirmez and Imran, 2003; Kolla et al., 2007) but very different preserved stratigraphic architecture due primarily to differences in channel aggradation during channel-belt evolution (Imran et al., 1998, 1999; Peakall et al., 2000; Jobe et al., 2016). Aggradation of the channel above the floodplain results in storage of potential energy in the flow to cause an avulsion (Imran et al., 1998; Mohrig et al., 2000). For river systems, this potential energy is high because of the large excess density between the flow (water) and the ambient fluid (air; Imran et al., 1998), resulting in rivers that can only reach 1 channel depth above the floodplain before avulsion (Mohrig et al., 2000). In submarine channel systems sculpted by turbidity currents, however, the potential energy is much lower due to the relatively small excess density between a turbidity current and the ambient seawater, leading to taller levees and less frequent avulsion (Imran et al., 1998).

In both rivers and submarine channels, avulsion is an important process for the construction of fluvial (Heller and Paola, 1996; Ganti et al., 2016) and submarine stratigraphic architecture (Flood et al., 1991; Torres et al., 1997; Schwenk et al., 2003). Avulsion is defined as the process by which flow is diverted out of an established channel belt into a new flow pathway on the adjacent floodplain (Mohrig et al., 2000; Slingerland and Smith, 2004). For avulsion to occur, the channel belt must aggrade above the adjacent floodplain to create a favorable potential energy gradient (i.e., the 'setup'; Bridge and Leeder, 1979; Bryant et al., 1995; Heller and Paola, 1996; Mohrig et al., 2000) and there must be a trigger/initiation event (Jones and Schumm, 1999). A channel belt is typically defined as the genetic deposits of one avulsion cycle (Leeder, 1978; Bridge and Leeder, 1979). River avulsions are well studied, and numerous avulsions have been observed during historic times (e.g., Smith et al., 1989). Avulsion setup criteria for rivers are well constrained (Mohrig et al., 2000; Ganti et al., 2016) and documented triggers are commonly levee breaches during floods (e.g., Slingerland and Smith, 1998,

2004). It is tempting for a specific event (e.g., a levee failure) to trigger avulsion, but simple overspill from a bankfull flow may be enough to generate channel avulsions (Edmonds et al., 2009), particularly when avulsion criteria have been reached.

In submarine channel systems, no historical avulsions have been observed or documented, and both the setup and triggering mechanisms are poorly constrained. Most work has focused not on the setup, but instead on interpreting triggers, which include flow-overspill and flow-stripping (Piper and Normark, 1983; Fildani et al., 2006), channel-floor aggradation (Kolla, 2007; Armitage et al., 2012), levee failure by mass-wasting (Flood et al., 1991), and mass-transport deposition/erosion (Ortiz-Karpf et al., 2015). Avulsion triggers are difficult to predict due to their dependence on local factors and their opportunistic nature (Slingerland and Smith, 2004); however, the setup can easily be measured and constrained using the abundant seafloor, seismic reflection, and core data that documents Quaternary avulsions in submarine channel systems (e.g., Pirmez and Flood, 1995; Manson, 2009 for the Amazon, Torres et al., 1997 for the Rhone). In this study, we document aggradation metrics and develop avulsion setup criteria for submarine channels. We also develop a theory for coupling between channels and their associated floodplains and explore differences between fluvial and submarine channel-floodplain coupling and the implications for channel-belt stability and avulsion frequency.


## Governing Equations

### *Superelevation*

The relative superelevation ($S_E$) is defined as the relief between the levee crest ($L_R$) and the adjacent floodplain normalized by the channel depth (H; Equation 1) (Bryant et al., 1995; Mohrig et al., 2000). Superelevation $S_E$ of the channel should not be confused with superelevation of the water/flow surface at the apex of a meander bend due to centrifugal acceleration (Dietrich and Whiting, 1989 for riverine flow; Hay et al., 1987 for turbidity currents).

*Equation 1, avulsion criterion for rivers using relative superelevation:* $S_E = \frac{L_R}{H}$

A superelevation $S_E = 1$ indicates that the channel is perched 1 channel depth above the floodplain; data from modern and ancient fluvial systems (Mohrig et al., 2000; Jerolmack, 2009) suggest this value is a practical maximum for rivers. An avulsion is imminent when the channel is superelevated one channel depth above the surrounding floodplain and only requires a trigger event. The rationale for this maximum value of $S_E$ is that by the time the channel thalweg reaches the elevation of the adjacent

floodplain ($S_E \sim 1$), there is sufficient potential energy for avulsion to take place (Imran et al., 1998; Mohrig et al., 2000).

Tall and thick levees and a channel perched high above the submarine floodplain have long been recognized in submarine channel systems (Buffington, 1952; Damuth and Flood, 1983; Hubscher et al., 1997) and explained by the flow properties of turbidity currents (Imran et al., 1998, 1999). Levee relief has also been documented for many submarine systems (e.g., Amazon Pirmez and Imran, 2003; Zaire Babonneau et al., 2010) and shown to be larger than that of rivers; however, superelevation and how it evolves through channel-belt evolution has never before been compiled for submarine systems, nor has a maximum $S_E$ value been proposed as an avulsion criteria for submarine channels.

## *Channel-floodplain coupling*

Superelevation theory for rivers (Equation 1; Mohrig et al., 2000) is useful for characterizing the modern geomorphological parameters. However, we are interested in the preserved record of channel-belt evolution and the potential coupling between the channel and its floodplain. Hence, we use parameters that can be measured from the preserved stratigraphic record to define a geometric equation that governs the amount of coupling between the channel and its floodplain in both fluvial and submarine systems (Fig. 1):

*Equation 2, Channel-floodplain coupling (fluvial and submarine):* $L_R = A_C - A_F$ , where $A_C = A_L$

This geometric coupling equation relates the aggradation of the levee and floodplain to the channel aggradation, where $L_R$ is levee relief, $A_C$ is channel aggradation, $A_F$ is floodplain aggradation, and $A_L$ is levee aggradation (Fig. 1). The necessary conditions to form this geometric relationship are: (1) channel depth H must be constant during channel evolution for $A_C$ and $A_L$ to be equal, (2) $L_R=0$ at channel initiation (Fig. 1), and (3) channels are net aggradational. We acknowledge that H is spatially and temporally variable in both fluvial (Nittrouer et al., 2011) and submarine (Shumaker et al., 2018) channels, but this assumption is made for simplicity. We also acknowledge that some channels do evolve through an incisional phase (e.g., Strong and Paola, 2008; Sylvester et al., 2011; Jobe et al., 2016), but this study is focused on aggradational channels that lack a significant incisional phase (e.g., the Amazon submarine system, Pirmez and Flood, 1995).

## **Channel-floodplain coupling in rivers**

In rivers, $A_F$ is considered negligible because channel-belt deposition ($A_C$, $A_L$) will be much more rapid than far-field, distal floodplain aggradation (Fig. 1; Wolman and Leopold, 1957; Leeder, 1978; Bridge and Leeder, 1979; Brizga and Finlayson, 1990; Jerolmack and Paola, 2007; Hajek and Edmonds, 2014). Numerous aggradation rate measurements from modern floodplains demonstrate this difference, with $A_C$ 10-55 times greater than $A_F$ (Pizzuto, 1987; Bridge and Leeder, 1979; Tornquist and Bridge, 2002; Jerolmack and Paola, 2007; Aalto et al., 2008). This indicates a very weak coupling between the channel and the floodplain for fluvial systems.

If $A_F = 0$, Equation 2 can be re-written as:

*Equation 3, Fluvial channel-floodplain coupling, where $A_F = 0$:   $A_C = L_R$*

We assume a simplified (i.e., flat) floodplain, while acknowledging that floodplain topography/dynamics (Lewin and Ashworth, 2014; Johnston et al., 2019) can affect avulsion location (Jerolmack and Paola, 2007) and avulsion style (Hajek and Edmonds, 2014). The theory in Equation 3 is also restricted to normal-flow fluvial reaches upstream of the backwater limit (the location where the mean elevation of the riverbed drops below sea-level or lake-level). In the backwater zone, the sediment-transport regime is modified by spatial and temporal flow non-uniformity, which affects channel-floor aggradation and scouring (Nittrouer et al., 2012), reduces levee growth and relief (Ganti et al., 2016), and changes channel belt dynamics and dimensions (Fernandes et al., 2016; Martin et al., 2018). Due to these complex hydro- and morpho-dynamics, this study will not further discuss coastal/backwater river systems, instead focusing on the differences between submarine channels and alluvial river reaches upstream of the backwater limit.

**Channel-floodplain coupling in submarine channels**

Floodplain aggradation $A_F$ is more significant in submarine channel settings when compared to channel aggradation $A_C$; rapid floodplain deposition is caused by hemipelagic deposition and overbanking dilute, sheet-like turbidity currents (Stow and Piper, 1984; Straub et al., 2008; Jobe et al., 2011). Unfortunately, datasets with paired in-channel and floodplain rate data do not exist, but several examples contain levee-crest data, demonstrating the importance of floodplain deposition in submarine systems. In the Bengal submarine channel, floodplain aggradation rates are ~50 cm/ky (core 120KL) when levee-crest aggradation rates are ~100 cm/ky (core 118KL, Weber et al., 1997). In the Amazon submarine channel, levee-crest aggradation rates are 360-517 cm/ky (sites 936, 946) while floodplain aggradation rates are 50-125 cm/ky (sites 930, 932, 935) (Mikkelsen et al., 1997). These two examples

indicate that $A_C$ is only 2-10 times greater than $A_F$, and thus $A_F$ cannot be neglected when considering channel-floodplain coupling (Fig. 1), and Equation 2 is modified accordingly:

*Equation 4, Submarine channel-floodplain coupling, where $A_F > 0$:* $\dfrac{A_C}{L_R} > 1$

This suggests that for a given channel dimension, submarine systems will be systematically thicker than a fluvial system due to a positive $A_F$ (Fig. 1) and greater levee relief (Buffington, 1952; Damuth and Flood, 1983). While Dorrell et al. (2015) demonstrate that submarine channels eventually become unstable and avulse due to geometric constraints when aggrading, we suggest that submarine channel-floodplain coupling is stronger than that in rivers, and as a result submarine channels are more stable than rivers under aggradational conditions (i.e., with $S_E > 1$, see Fig. 1). A compilation of data from rivers and submarine channel belts (Jobe et al., 2016) supports this hypothesis.

*Fig. 1. Fluvial and submarine channel-belt metrics for measuring aggradation and determining avulsion criteria. (A) Governing equations (see text for explanation of terms). (B) Fluvial channel-belt diagram and avulsion criteria. (B) Submarine channel diagram and avulsion criteria. Submarine channels can be up to 10 times thicker than rivers at avulsion due to enhanced superelevation and channel-floodplain coupling.*

## Channel-belt thickness: Combining superelevation and coupling parameters

Figure 1 shows the geometric relationships between the various measurable channel-belt parameters, and these can be arranged to define the thickness of the channel belt ($H_{CB}$) by relating the channel depth H and the aggradation of the channel $A_C$:

*Equation 5A, Channel-belt thickness for fluvial and submarine channels*     $H_{CB} = H + A_C$

*Equation 5B, Normalized channel-belt thickness* $\quad \frac{H_{CB}}{H} = 1 + \frac{A_C}{H}$

Because H tends to be quite variable between (and sometimes within) systems (Shumaker et al., 2018), normalized channel-belt thickness (Equation 5B′ also see Jobe et al., 2016) is preferred when comparing systems, and we will subsequently use this form.

By expanding the $A_C/H$ term in Equation 5B to include $L_R$, we obtain a more general form that defines channel-belt thickness using a dimensionless superelevation term and a dimensionless coupling term:

*Equation 6. Channel belt thickness* $\quad \frac{H_{CB}}{H} = 1 + \left(\frac{L_R}{H}\right)\left(\frac{A_C}{L_R}\right)$

We can further modify the $A_C/L_R$ term in Equation 6 by utilizing the relationship in Equation 2 to derive

*Equation 7. Channel-floodplain coupling parameter* $\quad \frac{A_C}{L_R} = \frac{A_C}{A_C - A_F} = \chi$

The parameter $\chi$ describes channel-floodplain coupling without using $L_R$ or H, which define the superelevation parameter $S_E$ (Equation 1). Substituting $\chi$ and $S_E$ into Equation 6, we can rewrite the final form of the channel-belt thickness equation as:

*Equation 8, Channel-belt thickness with superelevation and channel-floodplain coupling terms:*

$$\frac{H_{CB}}{H} = 1 + (S_E)(\chi)$$

Using Equation 8 and our understanding of channel-belt evolution and avulsion, we can estimate $H_{CB}$ when avulsion occurs for both fluvial and submarine systems.

**Fluvial conditions for avulsion**

Rivers have well-documented avulsions and the avulsion setup is well constrained (Bridge and Leeder, 1979; Smith et al., 1989). In particular, Mohrig et al. (2000) established a superelevation criteria for river avulsion, with $S_E \sim 1$ at avulsion. Under the condition where H remains constant through channel-belt construction, fluvial channels become unstable and are prone to avulse when $H = L_R = A_C = A_L$ (Fig. 1; Equation 1). Assuming $A_F = 0$ in fluvial systems (see discussion in Equation 3), the avulsion criteria for rivers can therefore be summarized as:

$$A_F \approx 0, \qquad S_E = 1, \qquad \chi = 1$$

Solving Equation 8 using these values, the normalized channel-belt thickness for a fluvial system at avulsion is 2 (i.e., $H_{CB}/H = 2$; also see Fig. 1). This is consistent with superelevation theory (Mohrig et al., 2000) as well as channel-floodplain coupling discussed above.

**Submarine conditions for avulsion**

For submarine channel belts, very little data has been collected on measurable parameters as compared to rivers. However, levee relief values are extremely large compared to channel depth in active channels (Damuth and Flood, 1983; Hubscher et al., 1997), suggesting that submarine channels are more stable at higher $S_E$ values than rivers (cf. Dorrell et al., 2015). Floodplain aggradation is significant (Mikkelsen et al., 1997; Weber et al., 1997) and cannot be ignored. Thus, we can summarize the avulsion criteria for submarine channels as:

$$A_F > 0, \quad S_E > 1, \quad \chi > 1$$

Hence, if we solve Equation 8 using these values, $H_{CB}/H > 2$ and potentially $\gg 2$ (Fig. 1). It is the aim of this paper to determine these values more precisely for submarine channel belts and quantify exactly how much more aggradational submarine channels are than rivers prior to avulsion.

# Data collection methodology

Coupling between the channel and the floodplain for any channelized setting can be described by measuring three channel-belt parameters: the levee relief above the floodplain $L_R$, the aggradation of the channel $A_C$, and the aggradation of the floodplain $A_F$ (Fig. 1). These parameters were measured from a compilation of 52 cross sections from the Amazon, Zaire, Danube, Rhone, Magdalena, and Mississippi submarine channels (Table 1). Our methods for objectively defining the levee crest, channel thalweg, floodplain elevation, and channel-belt base are described here and in Fig. 1. The levee crest and channel thalweg are straightforward to define by using the highest and lowest point, respectively, on a cross-sectional profile of the seafloor (Fig. 1). The channel-belt base can be defined as the initial location of the channel at the beginning of channel-belt deposition (i.e., the first location of the channel post-avulsion) and is typically straightforward to locate using a seismic reflection profile across the channel (Fig. 2). Where picking the channel-belt base was ambiguous, we selected the lowest point of the interpreted channel belt (Fig. 1, Fig. 2). The most subjective and interpretive data to collect is the floodplain elevation (i.e., the base of the levee). The location of this point can be difficult to define, given that levee relief decreases asymptotically towards the floodplain in rivers (Pizzuto, 1987;

Ferguson and Brierley, 1999) and submarine channels (Normark et al., 1993; Skene et al., 2002; Straub and Mohrig, 2008; Nakajima and Kneller, 2012). We tested various methods to define the floodplain elevation, including (1) a levee-slope derivative, (2) a levee-slope inflection point, and (3) fitting of power law and/or exponential equations to the levee slope. However, these methods can generate spurious results due to variations in data quality and local factors that affect the levee such as sediment waves, gullies, faults, and older/younger channel belts on the levee (Nakajima and Kneller, 2012). Hence, we select the floodplain elevation qualitatively (i.e., via 'ocular inspection'), constraining this location according to two criteria: (1) where the levee slope has an inflection, and (2) where the channel belt thickness stabilizes (Fig. 1, Fig. 2; cf. Jerolmack and Paola, 2007). Generally, these two criteria are spatially correlated, and while we recognize this qualitative method has inherent uncertainty, given general data quality and complexity of antecedent topographies it does not appear to be possible to define the floodplain elevation in a more rigorous, quantitative manner (also see discussion in Normark et al., 1993).

Cross sections in our compilation were selected to (1) include extant channels on the seafloor (i.e., not buried or compacted), (2) not be affected by large faults or other allogenic factors, and (3) be approximately perpendicular to the channel so that measurements of channel and channel-belt dimensions are accurate (i.e., no artificially wide channels due to oblique cross sections). If the cross-section had two-way travel time as the vertical unit, we converted to meters using a seawater velocity of 1500 m/s (i.e., 100 ms TWT = 75 m). While the shallow subsurface often has velocities 1400-2000 m/s (e.g., Flood et al., 1997), and we realize that using 1500 m/s may slightly underestimate subsurface thickness, it more accurately represents the seafloor surface, which is important for our calculations of $L_R$ and H. From the scaled cross-sections (examples in Fig. 2), we created the following:

- a line trace of the seafloor (upper black line in Fig. 1, Fig. 2)
- a line trace of the base of the channel belt (lower black line in Fig. 1, Fig. 2)
- 2 points marking the location of the levee crests (red dots in Fig. 1, Fig. 2)
- 2 points marking the location of the floodplain elevation (blue dots in Fig. 1, Fig. 2)
- 1 point marking the initial location of the channel-base (green dot in Fig. 1, Fig. 2)

Two values of $L_R$ are calculated (as shown in Fig. 1) as the vertical distance between each levee crest points and the floodplain elevation; those two values are averaged into the final value of $L_R$. Two values of $A_F$ are also calculated as the vertical distance between the floodplain elevation and the line defining the channel-belt base (Fig. 1); again, those two values are averaged into the final value of $A_F$. We average the two values of $L_R$ and $A_F$ rather than take a maximum or minimum value because of local

variations in levee morphology and variations in data quality (Fig. 2). For example, the cross-section in Figure 2A is not exactly perpendicular to the flow direction of the channel, causing a slight elevation difference between the two floodplains, and an average of the two measurements somewhat alleviates this issue. The channel aggradation $A_C$ is calculated as the vertical distance between the point marking the initial location of the channel and the channel thalweg (defined as the minimum y value of the line trace of the seafloor between the levee crests; Fig. 1). Examples of typical seismic-reflection profiles are shown in Fig. 2.
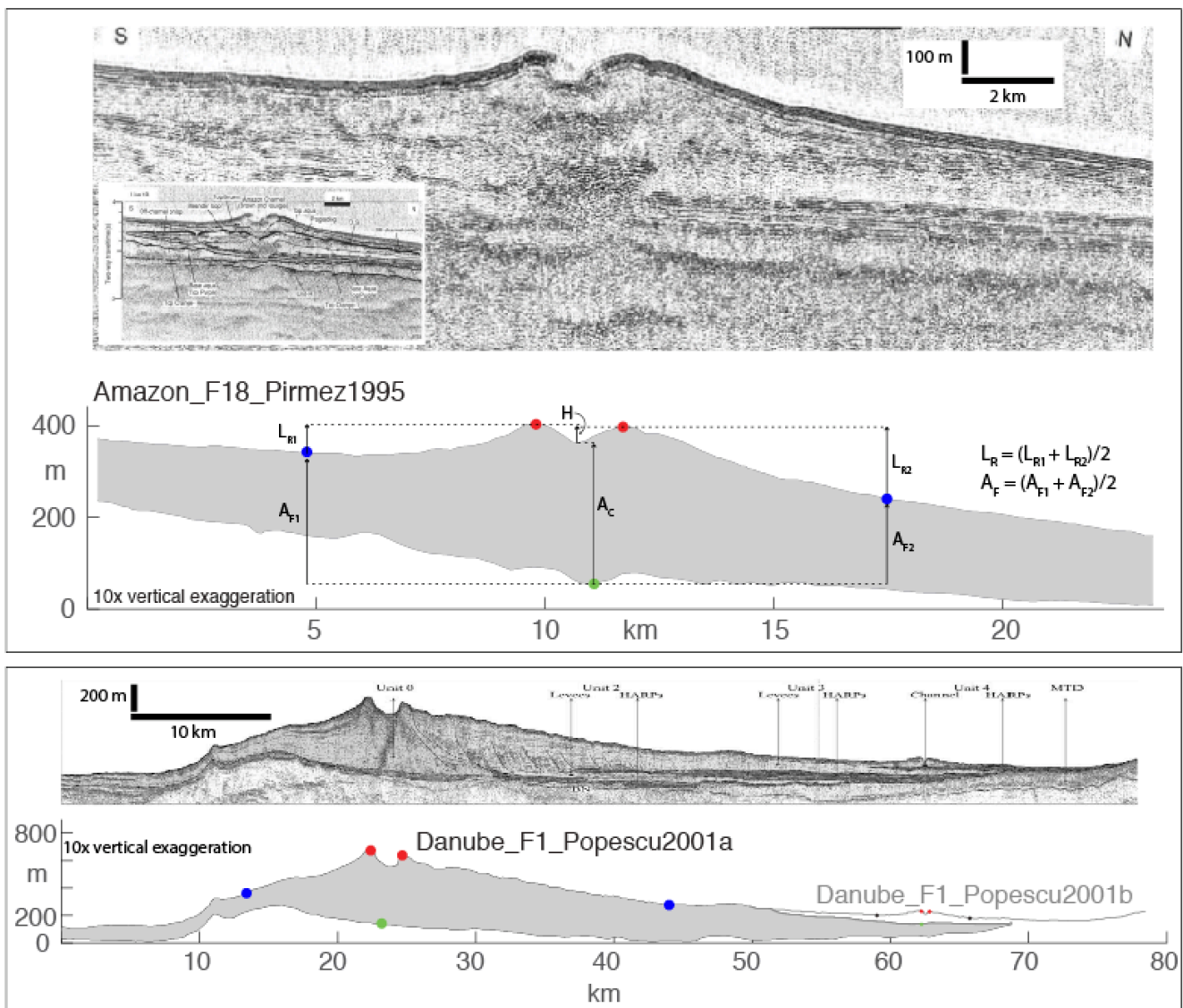


Fig. 2. Seismic-reflection profiles and associated measurements of the Amazon channel (A) and Danube channel (B). Both profiles displayed at 10x vertical exaggeration but are not scaled to each other. Note the significant aggradation of the channel above the floodplain in both channels. Note also the

*difference in superelevation between the Danube abandoned channel (left) and the modern channel (right). Image in (A) from Pirmez and Flood (1995); image in (B) from Popescu et al. (2001).*

# Results

Fifty-two submarine channel belts are shown in Fig. 3, with channel-base, levee crests, and floodplain elevations indicated in green, red, and blue, respectively. These data are derived from the modern and Quaternary channels of the following submarine fans: Amazon (n=35; key reference is Manson (2009)), Zaire (n=9; Picot et al. (2016)), Danube (n=3; Popescu et al. (2001)), Rhone (n=3; Bonnel et al. (2005)), Magdalena (n=1; Leslie et al. (2011)), and Mississippi (n=1; Stelting et al. (1986)). Channel dimensions are consistent with other data compilations from submarine systems (Table 1; Konsoer et al., 2013; Shumaker et al., 2018), providing confidence in our data collection methodology.
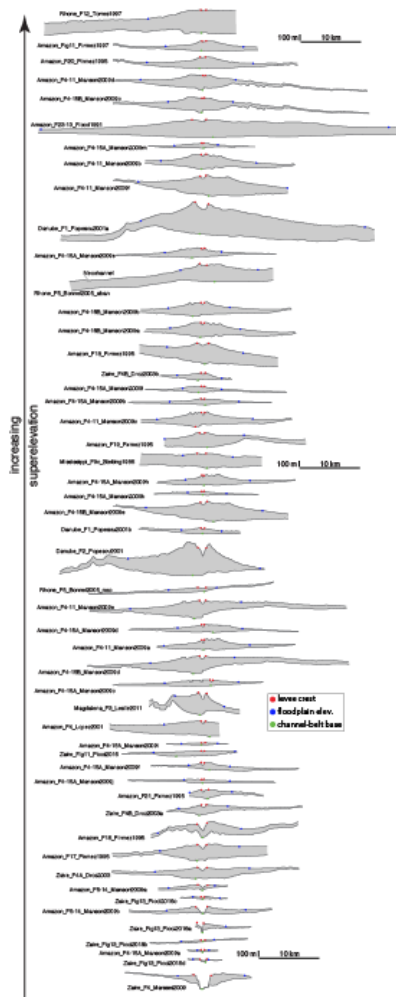
| Name | System | Source | width (m) | depth (m) | Hcb (m) | levee relief (m) | floodplain aggradation (m) | channel aggradation (m) | superelevation | coupling parameter | uniqueID |
|---|---|---|---|---|---|---|---|---|---|---|---|
| Amazon_F23-13_Flood1991 | Amazon | Flood et al. 1991 | 2353 | 33 | 290 | 146 | 92 | 257 | 4.42 | 1.56 | 7 |
| Amazon_F23-2A_Flood1991 | Amazon | Flood et al. 1991 | 2685 | 147 | 498 | 172 | 331 | 350 | 1.17 | 18.42 | 52 |
| Amazon_F4_Lopez2001 | Amazon | Lopez, 2001 | 758 | 42 | 256 | 55 | 152 | 213 | 1.31 | 3.49 | 29 |
| Amazon_F4-11_Manson2009a | Amazon | Manson 2009 thesis | 409 | 59 | 163 | 91 | 41 | 103 | 1.54 | 1.66 | 8 |
| Amazon_F4-11_Manson2009b | Amazon | Manson 2009 thesis | 814 | 35 | 245 | 125 | 71 | 210 | 3.57 | 1.51 | 9 |
| Amazon_F4-11_Manson2009c | Amazon | Manson 2009 thesis | 537 | 43 | 235 | 108 | 71 | 192 | 2.51 | 1.59 | 10 |
| Amazon_F4-11_Manson2009d | Amazon | Manson 2009 thesis | 384 | 11 | 243 | 71 | 53 | 231 | 6.45 | 1.30 | 11 |
| Amazon_F4-11_Manson2009e | Amazon | Manson 2009 thesis | 1026 | 52 | 300 | 84 | 74 | 248 | 1.62 | 1.43 | 12 |
| Amazon_F4-11_Manson2009f | Amazon | Manson 2009 thesis | 950 | 43 | 330 | 149 | 58 | 286 | 3.47 | 1.25 | 13 |
| Amazon_F4-15A_Manson2009a | Amazon | Manson 2009 thesis | 555 | 40 | 40 | 6 | 22 | 0 | 0.15 | 0.00 | 14 |
| Amazon_F4-15A_Manson2009b | Amazon | Manson 2009 thesis | 540 | 17 | 98 | 44 | 26 | 81 | 2.59 | 1.47 | 15 |
| Amazon_F4-15A_Manson2009c | Amazon | Manson 2009 thesis | 449 | 29 | 93 | 41 | 38 | 63 | 1.41 | 2.52 | 16 |
| Amazon_F4-15A_Manson2009d | Amazon | Manson 2009 thesis | 424 | 36 | 127 | 57 | 51 | 91 | 1.58 | 2.28 | 17 |
| Amazon_F4-15A_Manson2009e | Amazon | Manson 2009 thesis | 457 | 18 | 152 | 61 | 66 | 134 | 3.39 | 1.97 | 18 |
| Amazon_F4-15A_Manson2009f | Amazon | Manson 2009 thesis | 520 | 44 | 121 | 52 | 53 | 77 | 1.18 | 3.21 | 19 |
| Amazon_F4-15A_Manson2009h | Amazon | Manson 2009 thesis | 337 | 35 | 164 | 80 | 61 | 129 | 2.29 | 1.90 | 20 |
| Amazon_F4-15A_Manson2009i | Amazon | Manson 2009 thesis | 618 | 10 | 34 | 12 | 12 | 23 | 1.20 | 2.09 | 21 |
| Amazon_F4-15A_Manson2009j | Amazon | Manson 2009 thesis | 372 | 14 | 62 | 15 | 28 | 48 | 1.07 | 2.40 | 22 |
| Amazon_F4-15A_Manson2009k | Amazon | Manson 2009 thesis | 387 | 12 | 59 | 25 | 25 | 46 | 2.08 | 2.19 | 23 |
| Amazon_F4-15A_Manson2009l | Amazon | Manson 2009 thesis | 489 | 15 | 101 | 41 | 34 | 85 | 2.73 | 1.67 | 50 |
| Amazon_F4-15A_Manson2009m | Amazon | Manson 2009 thesis | 302 | 10 | 84 | 36 | 32 | 73 | 3.60 | 1.78 | 51 |
| Amazon_F4-15B_Manson2009a | Amazon | Manson 2009 thesis | 527 | 32 | 237 | 96 | 91 | 204 | 3.00 | 1.81 | 24 |
| Amazon_F4-15B_Manson2009b | Amazon | Manson 2009 thesis | 548 | 27 | 226 | 86 | 98 | 199 | 3.19 | 1.97 | 25 |
| Amazon_F4-15B_Manson2009c | Amazon | Manson 2009 thesis | 370 | 13 | 242 | 66 | 86 | 228 | 5.08 | 1.61 | 26 |
| Amazon_F4-15B_Manson2009d | Amazon | Manson 2009 thesis | 1026 | 51 | 295 | 71 | 99 | 244 | 1.39 | 1.68 | 27 |
| Amazon_F4-15B_Manson2009e | Amazon | Manson 2009 thesis | 1086 | 45 | 326 | 93 | 60 | 280 | 2.07 | 1.27 | 28 |
| Amazon_F16_Pirmez1995 | Amazon | Pirmez and Flood 1995 | 1647 | 123 | 232 | 120 | 77 | 109 | 0.98 | 3.41 | 1 |
| Amazon_F17_Pirmez1995 | Amazon | Pirmez and Flood 1995 | 1533 | 69 | 270 | 67 | 106 | 200 | 0.97 | 2.13 | 2 |
| Amazon_F18_Pirmez1995 | Amazon | Pirmez and Flood 1995 | 1879 | 37 | 345 | 110 | 186 | 307 | 2.97 | 2.54 | 3 |
| Amazon_F19_Pirmez1995 | Amazon | Pirmez and Flood 1995 | 854 | 26 | 238 | 66 | 88 | 211 | 2.54 | 1.72 | 4 |
| Amazon_F20_Pirmez1995 | Amazon | Pirmez and Flood 1995 | 896 | 15 | 188 | 96 | 48 | 172 | 6.40 | 1.39 | 5 |
| Amazon_F21_Pirmez1995 | Amazon | Pirmez and Flood 1995 | 1174 | 41 | 150 | 42 | 48 | 109 | 1.02 | 1.79 | 6 |
| Amazon_Fig11_Pirmez1997 | Amazon | Pirmez et al. 1997 | 685 | 14 | 159 | 90 | 52 | 144 | 6.43 | 1.57 | 32 |
| Danube_F1_Popescu2001a | Danube | Popescu et al. 2001 | 2242 | 101 | 509 | 347 | 177 | 408 | 3.44 | 1.77 | 33 |
| Danube_F1_Popescu2001b | Danube | Popescu et al. 2001 | 571 | 20 | 88 | 38 | 43 | 68 | 1.90 | 2.72 | 34 |
| Danube_F2_Popescu2001 | Danube | Popescu et al. 2001 | 1395 | 140 | 459 | 262 | 105 | 318 | 1.87 | 1.49 | 35 |
| Magdalena_F3_Leslie2011 | Magdalena, Colombia | Leslie et al. 2012 | 1393 | 100 | 364 | 137 | 90 | 264 | 1.37 | 1.52 | 36 |
| Mississippi_F9c_Stelting1986 | Mississippi | Stelting et al. 1986 | 1485 | 19 | 244 | 46 | 175 | 225 | 2.42 | 4.50 | 37 |
| Rhone_F5_Bonnel2005_aban | Rhone | Bonnel et al. 2005 | 1165 | 27 | 288 | 92 | 179 | 260 | 3.41 | 3.21 | 39 |
| Rhone_F5_Bonnel2005_neo | Rhone | Bonnel et al. 2005 | 1360 | 11 | 68 | 20 | 31 | 56 | 1.82 | 2.24 | 38 |
| Rhone_F12_Torres1997 | Rhone | Torres et al. 1997 | 883 | 19 | 380 | 147 | 212 | 361 | 7.74 | 2.42 | 40 |
| Zaire_F4A_Droz2003 | Zaire | Dorz et al. 2003 | 1573 | 54 | 185 | 41 | 65 | 131 | 0.76 | 1.98 | 42 |
| Zaire_F4B_Droz2003a | Zaire | Dorz et al. 2003 | 785 | 39 | 174 | 41 | 51 | 134 | 1.05 | 1.61 | 43 |
| Zaire_F4B_Droz2003b | Zaire | Dorz et al. 2003 | 722 | 23 | 122 | 65 | 25 | 98 | 2.83 | 1.34 | 44 |
| Zaire_F5-14_Manson2009a | Zaire | Manson 2009 thesis | 1663 | 47 | 86 | 28 | 31 | 38 | 0.60 | 5.43 | 30 |
| Zaire_F5-14_Manson2009b | Zaire | Manson 2009 thesis | 1906 | 104 | 109 | 56 | 41 | 5 | 0.54 | -0.14 | 31 |
| Zaire_F4_Marsset2009 | Zaire | Marsset et al. 2009 | 2893 | 233 | 233 | 8 | 45 | 0 | 0.03 | 0.00 | 41 |
| Zaire_Fig11_Picot2016 | Zaire | Picot et al. 2016 | 548 | 14 | 89 | 18 | 16 | 74 | 1.29 | 1.28 | 45 |
| Zaire_Fig13_Picot2016a | Zaire | Picot et al. 2016 | 1099 | 162 | 162 | 62 | 22 | 0 | 0.38 | 0.00 | 46 |
| Zaire_Fig13_Picot2016b | Zaire | Picot et al. 2016 | 615 | 16 | 22 | 6 | 16 | 5 | 0.38 | -0.45 | 47 |
| Zaire_Fig13_Picot2016c | Zaire | Picot et al. 2016 | 526 | 12 | 32 | 6 | 17 | 20 | 0.50 | 6.67 | 48 |
| Zaire_Fig13_Picot2016d | Zaire | Picot et al. 2016 | 1129 | 31 | 48 | 2 | 8 | 17 | 0.06 | 1.89 | 49 |

Table 1. Parameters for fifty-two cross sections of submarine channel belts used in this study.

As a proxy for sediment volume encompassed in the channel belt, we calculated the area of each channel-belt cross-section (Fig. 4). These values are normalized by channel cross-sectional area, and the $P_{10}$-$P_{50}$-$P_{90}$ distribution of channel-belt area is 11-84-249 channel areas. This suggests that a typical submarine channel-belt (grey area in Fig. 3) contains 80-100 times the volume of sediment in the cross-section of the modern channel at the same streamwise location (Fig. 4). Values of fluvial channel belt area (or volume) are not available for comparison, but the channel belt data from Jobe et al. (2016) suggests that while rivers are much less aggradational, they build much wider channel belts than submarine channels; thus, both environments may have similar channel belt area values.
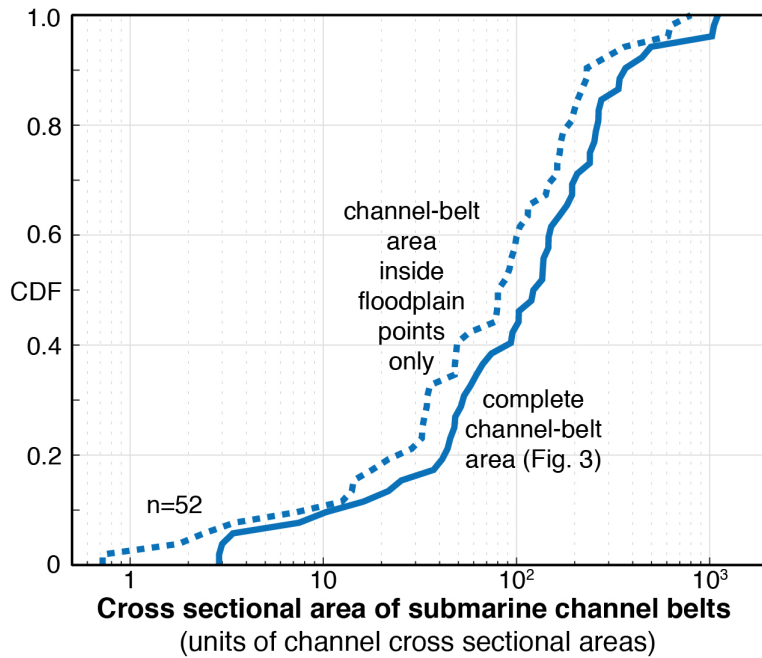
*Fig. 4. Cross-sectional area of submarine channel belts derived from cross sections in Figure 3. The solid line incorporates the full gray area from each channel belt in Figure 3, and the dashed line takes only the area within the floodplain points. No fluvial data are available for comparison, but channel belt aspect ratio data suggests that fluvial channel belts may have a similar distribution (see text).*

To enable comparison between channel-belt parameters, we compiled data from other submarine and fluvial systems. Jobe et al. (2016) provided values of normalized channel belt thickness ($H_{cb}/H$) from submarine and fluvial systems, and Mohrig et al. (2000) supplied values of superelevation ($S_E$) for fluvial systems (Fig. 5). Submarine systems have ~ 10 times thicker channel belts (Fig. 5), supporting the theory developed above as well as qualitative (e.g., Peakall et al., 2000; Kolla et al., 2007) and quantitative (Jobe et al., 2016) observations. Values of submarine $H_{cb}/H$ collected in this study are very similar to compiled data from other studies (Fig. 5), an encouraging result that supports our data collection methodology. However, our $H_{cb}/H$ values are slightly larger, likely because we focused solely on leveed, aggradational submarine channel belts, whereas Jobe et al. (2016) collected data from both erosional and constructional submarine channel belts.
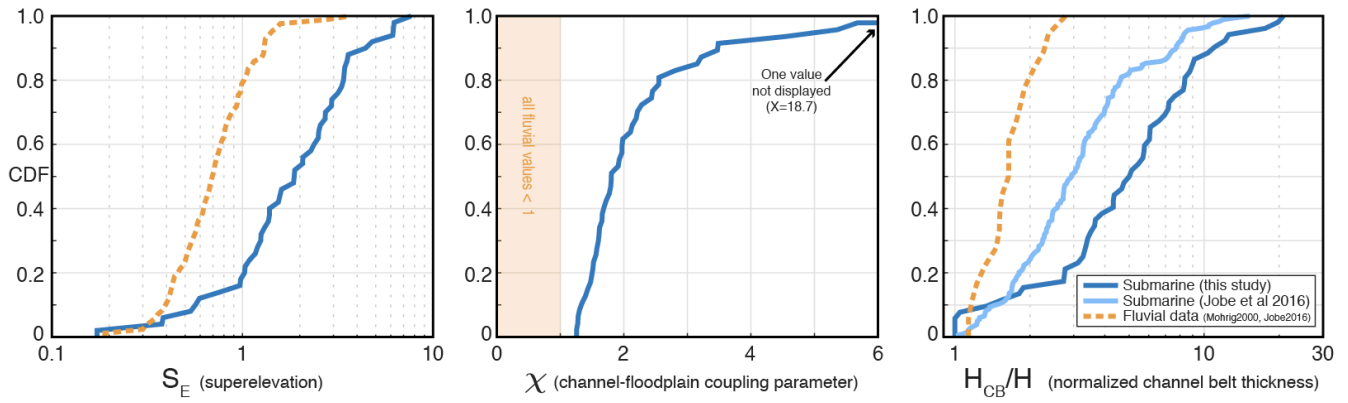
*Fig. 5. Comparisons of fluvial and submarine channel-belt parameters superelevation (A), χ coupling parameter (B), and normalized channel-belt thickness (C). In all cases, submarine channels show evidence for more aggradation and superelevation. These metrics suggest that avulsion criteria are very different for submarine and fluvial environments.*

The magnitude of levee relief $L_R$ for submarine channel-belts ($P_{50}$ of 64 m) is 10 to 70 times larger than fluvial channel-belt $L_R$ ($P_{50}$ of 1 m from Mohrig et al. 2000). Some larger rivers can have taller levees; for example, the Mississippi river has 6 m high levees (Shen et al., 2015) and the Rhine-Meuse system has 3-5 m high levees (Tornqvist, 1994). However, we cannot find an example of a fluvial levee > 10 m high, so an average submarine levee is still an order of magnitude taller than an average fluvial levee. This comparison is not normalized, and it is well documented that submarine channels are larger than rivers (Konsoer et al., 2013). Normalizing levee relief by channel depth (Equation 1; Mohrig et al., 2000) produces superelevation ($S_E$), which is shown in Fig. 5. We find that submarine channel $S_E$ values have a $P_{10-50-90}$ distribution of 0.8/1.9/4.5, while fluvial $S_E$ values are consistently lower, with a distribution of 0.4/0.7/1.3 (Fig. 5). From these distributions, submarine $S_E$ values are 1.2 to 3.5 times larger than fluvial $S_E$ values (Fig. 5), suggesting that submarine channels can be stable when superelevated up to 3.5 channel depths above the floodplain, while rivers nearly always avulse before reaching 1 channel depth of superelevation.

No published values of paired $A_F$ and $A_C$ values from fluvial systems were available to compute $\chi$ to compare to submarine values (Fig. 5). However, ratios of floodplain-aggradation to channel-aggradation *rates* range from 0.02 to 0.25 for rivers (Fig. 6; Allison et al., 1998; Makaske et al., 2002; Tornquist and Bridge, 2002; Aalto et al., 2008). While aggradation-rate data from submarine systems would be best for comparison, no reliable data exists. Hence, we simply compare the submarine $A_F/A_C$ ratio (from thickness data) to the fluvial $A_F/A_C$ ratio (from rate data), with the assumption that the larger values should most closely align with avulsion conditions (Fig. 6). The submarine $P_{90}$ and fluvial $P_{10}$

values of $A_F/A_C$ do not overlap (Fig. 6), supporting the avulsion criteria discussed above, specifically: (1) $A_F$ in fluvial systems is insignificant compared to $A_C$ and thus can be ignored when considering avulsion criteria for rivers (see Equation 3; Fig. 1) and (2) that $A_F$ cannot be ignored in submarine channel belts and thus must be included in the avulsion criteria (see Equation 4; Fig. 1). We caution that while these $A_F/A_C$ results are intuitive and consistent with theory and available data, they should be considered preliminary until $A_F/A_C$ rate data can be collected from submarine channel belts.
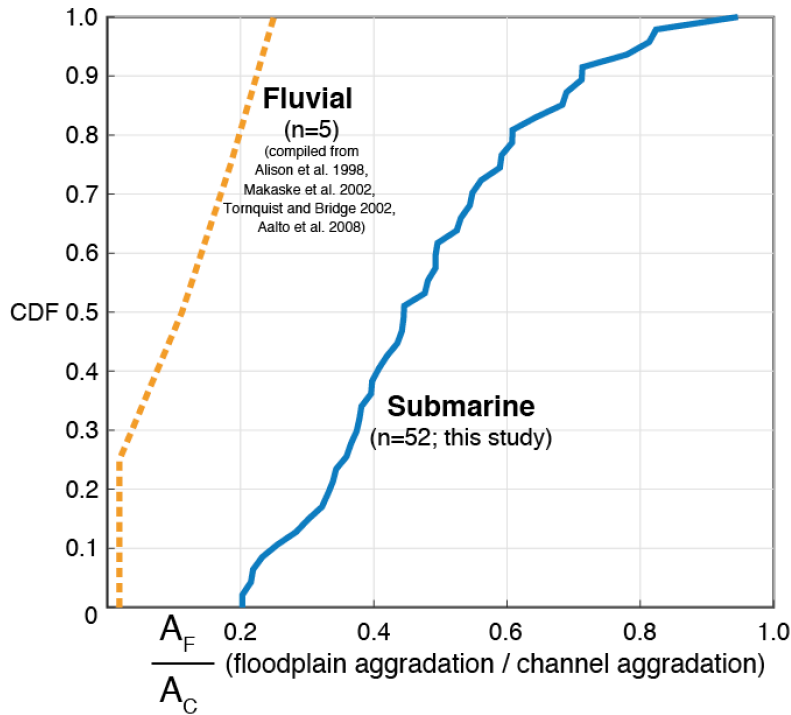


*Fig. 6. Ratio between channel aggradation and floodplain aggradation in fluvial and submarine channel systems. This relationship suggests that the relative contribution of floodplain aggradation is much more important in submarine channel belt growth, supporting the formulation of Equation 3 and Equation 4.*

## Discussion

### *Why are submarine channel belts so thick and superelevated?*

The results of this study clearly demonstrate that submarine channels commonly attain $S_E$ and $\chi$ > 1 (Fig. 5), values much higher than observed in fluvial systems. We interpret that the unique turbidity current flow properties in submarine channels are responsible for the significant superelevation and

aggradation of submarine channel-belts. Flows in submarine channels have ~50 times less density contrast between the flow and ambient fluid than rivers (Imran et al., 1998). This promotes higher sediment concentration in the upper portion of the flow, leading to levee and floodplain aggradation caused by enhanced overspill and flow stripping, particularly around channel bends (Piper and Normark, 1983; Hiscott et al., 1997). In addition, turbidity currents are strongly vertically stratified and the velocity maximum is located much closer to the bed than in a riverine flow (Sequeiros et al., 2010; Dorrell et al., 2014; Azpiroz-Zabala et al., 2017). This vertical stratification limits the potential for avulsion because: (1) the dense, energetic, coarse-grained portion of the flow remains near the channel thalweg rather than near the levee crest (Jobe et al., 2017), and (2) the top of the flow has very low sediment concentration and density contrast with the ambient fluid (Imran et al., 1998) and thus little to no driving force for erosion as compared to rivers (Konsoer et al., 2013), suggesting there is diminished ability for turbidity currents to erode the levee and trigger an avulsion. Collectively, these factors cause flows in submarine channels to have lower potential energy as compared to rivers (Imran et al., 1998; Mohrig et al., 2000). Therefore, submarine channels can attain larger values of levee relief, superelevation, and channel belt thickness prior to avulsion.

Submarine channel systems also have much greater floodplain aggradation than rivers (Fig. 6), likely because of two major sources of sediment: (1) overspill and flow-stripping from turbidity currents (Hiscott et al., 1997), which can occur at the rate of 0.3 overspill events per year (Piper and Deptuck, 1997), resulting in rapid floodplain aggradation, and (2) hemipelagic sedimentation, which is ubiquitous in submarine environments and can be very rapid (10-40 cm/ky) in high sediment-supply regimes where leveed submarine channels are common (Mikkelsen et al., 1997; Stow et al., 2001). The combination of muddy turbidity currents and hemipelagic deposition produces facies with rhythmically alternating very thin silt turbidite beds and bioturbated hemipelagic clay, which has been documented from many modern (e.g., Amazon channel Site 930, Hiscott et al., 1997, Normark and Damuth, 1997) and ancient floodplain settings (summarized in Hansen et al., 2017).

### *Criteria for submarine channel avulsion*

The theory and results demonstrated above allow us to develop avulsion criteria for submarine channels. Using Equation 8, these criteria should consist of a maximum value of $S_E$ and $\chi$ that creates a maximum $H_{CB}/H$. For rivers, the avulsion criteria are $S_E = 1$, $\chi = 1$, and $H_{CB}/H = 2$ (see section above "Fluvial conditions for avulsion"). We know that since the majority of $H_{CB}/H$ values for submarine

systems are greater than 2 (Fig. 5), avulsion values of $S_E$ and $\chi$ must be $\gg 1$. Using the distribution of fluvial $S_E$ values shown in Fig. 5, $S_{E\ fluvial} = 1$ occurs at the $P_{80}$ position of the distribution; Mohrig et al. (2000) suggest that while 1 is the practical avulsion threshold, some rivers can attain a slightly higher superelevation before avulsing. Using this reasoning, we can use the $P_{80}$ as a proxy for what the $S_E$ value should be at avulsion in a submarine channel system; again using Fig. 5, the $P_{80}$ $S_{E\ submarine} = 3.4$. Using the same reasoning for $\chi$, the $P_{80}$ submarine $\chi$ value is 2.5 (Fig. 5). Revisiting Equation 8, we can compute the value of $H_{CB}/H$ for submarine channel systems at avulsion:

$$S_E \sim 3.4, \qquad \chi \sim 2.5, \qquad \frac{H_{CB}}{H} = 1 + (S_E)(\chi), \qquad \rightarrow \qquad \frac{H_{CB}}{H} = 9.5 \ at \ avulsion$$

These avulsion thresholds are derived from our worldwide compiled dataset (n=52), but it is important to note that these values (particularly $H_{CB}/H$) likely vary from system to system based on slope position, the average excess density of flows, Froude number and vertical position of the velocity maximum (Sequeiros et al., 2010), and other factors not discussed here. For example, a system with higher excess density flows are likely associated with lower $S_E$ and $\chi$ values, leading to more rapid avulsion prior to attaining $H_{CB}/H \sim 9.5$.

To test the validity of these avulsion criteria, we construct a simple model of Equation 8 that calculates $H_{CB}/H$ from any value of $S_E$ and $\chi$ (colored lines in Fig. 7A). The independently measured $H_{CB}/H$ values from this study (black dots and red numbers in Fig. 7A) agree very well with the modeled $H_{CB}/H$ values derived using Equation 8. To quantify this agreement, Fig. 7B cross plots the measured $H_{CB}/H$ values (method defined in Fig. 1, Fig. 2) to the $H_{CB}/H$ values calculated using Equation 8. Although there is variability, Equation 8 is accurately predicting the observed values, with a coefficient of determination ($R^2$) of 0.40
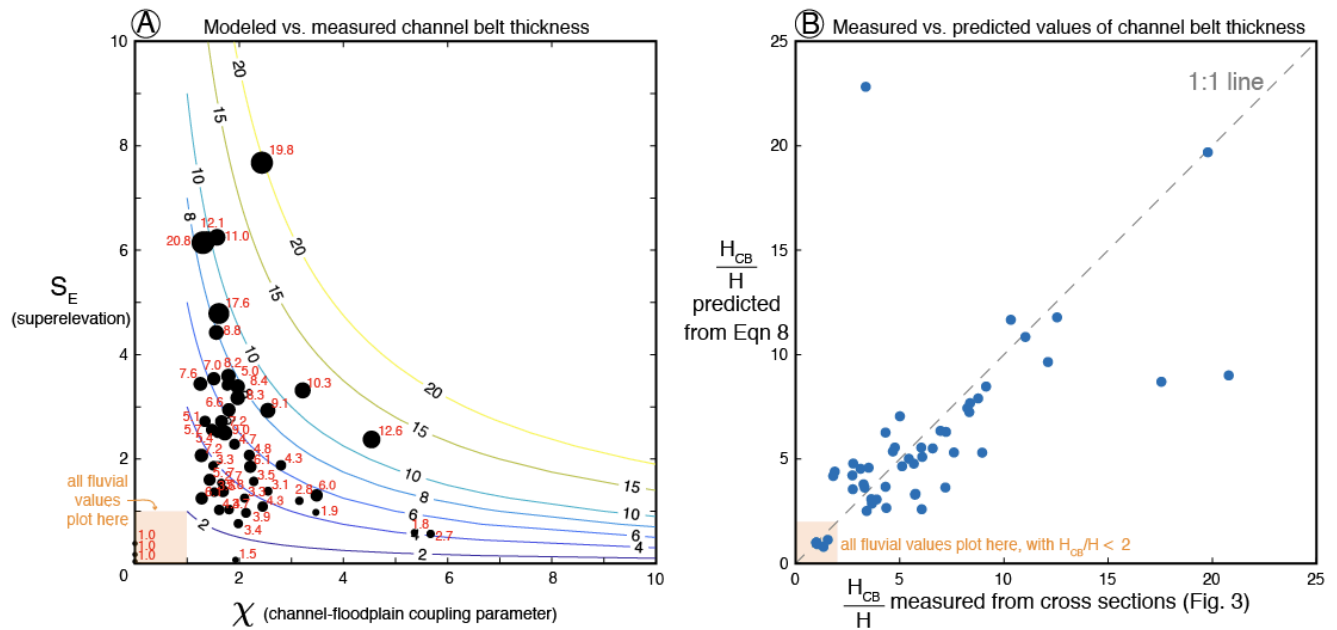
.

*Fig. 7. Comparing normalized channel-belt thickness ($H_{CB}/H$) values measured from submarine channel cross sections to values of $H_{CB}/H$ modeled using Equation 8 from this study. Note in both plots the position of fluvial values. (A) Plot of $S_E$ vs $\chi$, with colored contour lines showing $H_{CB}/H$ computed using Equation 8 and the black bubbles and red text indicating the measured $H_{CB}/H$ values. $P_{80}$ values of $S_E$ rarely exceeds 3.4 and $P_{80}$ $\chi$ values rarely exceed 2.5. (B) Plot of measured $H_{CB}/H$ values against computed $H_{CB}/H$ values using Equation 8. There is good agreement between measured and computed values of submarine $H_{CB}/H$. Also note that the avulsion threshold for submarine channels is approximately $H_{CB}/H = 9.5$; the majority of this study's data plots below this threshold.*

## Comparison to modern seafloor data

This study has focused on seismic-reflection data, where the base of the channel-belt can be confidently mapped (e.g., Fig. 2). However, there is a wealth of publicly available bathymetry data where the concepts presented here can be observed. Three passive-margin and four active-margin systems with easily accessible bathymetry data were chosen: Amazon (Pirmez and Imran, 2003), Bengal (Schwenk et al., 2003; Kolla et al., 2012), Joshua (Posamentier, 2003), and New Zealand systems (Hikurangi, Bounty, Haast, and Hokitika; Mountjoy et al., 2009). While the Amazon and New Zealand

systems have bathymetry coverage over most of their channel lengths, only the middle portion of the Joshua channel and the distal portion of the Bengal channel are imaged (Shumaker et al., 2018).

Fig. 8A displays bathymetry-based cross-sections of the Joshua, Amazon, Bengal, and Hikurangi submarine channels, and Fig. 8B quantifies $S_E$ values for all seven mapped systems. Passive-margin systems (Amazon, Joshua, Bengal) show larger values of $S_E$ and simpler seafloor topography, while active-margin systems have entrenched channels, low values of $S_E$, and more complex seafloor topography (Fig. 8A). The Amazon channel shows high levee relief ($L_R$) that decreases downstream, consistent previous observations (e.g., Damuth and Flood, 1983; Pirmez and Imran, 2003; Shumaker et al., 2018) and our compiled data (see next section and Fig. 9, Fig. 10). The Amazon and Joshua channels have very large values of $S_E$, up to almost 6 (Fig. 8B), consistent with their aggradational, avulsive nature (Damuth et al., 1983; Posamentier, 2003) and slope position. Since only the distal portion and channel mouth of the studied Bengal channel has bathymetry coverage (Shumaker et al., 2018), values of $S_E$ are small (Fig. 8B), but more proximal data shows a more aggradational channel similar to the Joshua and Amazon (Weber et al., 1997; Schwenk and Spiess, 2009). All four of the active-margin systems near New Zealand (Fig. 8) have high-relief submarine topography near the channel and thus are variably incised/entrenched (Fig. 8A). Values of $S_E$ for the four active-margin systems are $\ll 1$ and do not change predictably downslope (Fig. 8). We interpret that this difference is caused chiefly by the tectonic setting and associated seafloor deformation. While the Joshua, Amazon, and Bengal channels can build an equilibrium profile and thus have strong channel-floodplain coupling, and can aggrade a channel belt to the avulsion thresholds, the abundant seafloor topography in the Hikurangi, Haast, Bounty, and Hokitika channels creates a disequilibrium slope that perturbs the channel-floodplain coupling (Fig. 8). Hence, these active-margin channels are less likely to reach avulsion threshold values of $S_E$ and $\chi$ than passive-margin submarine channels.
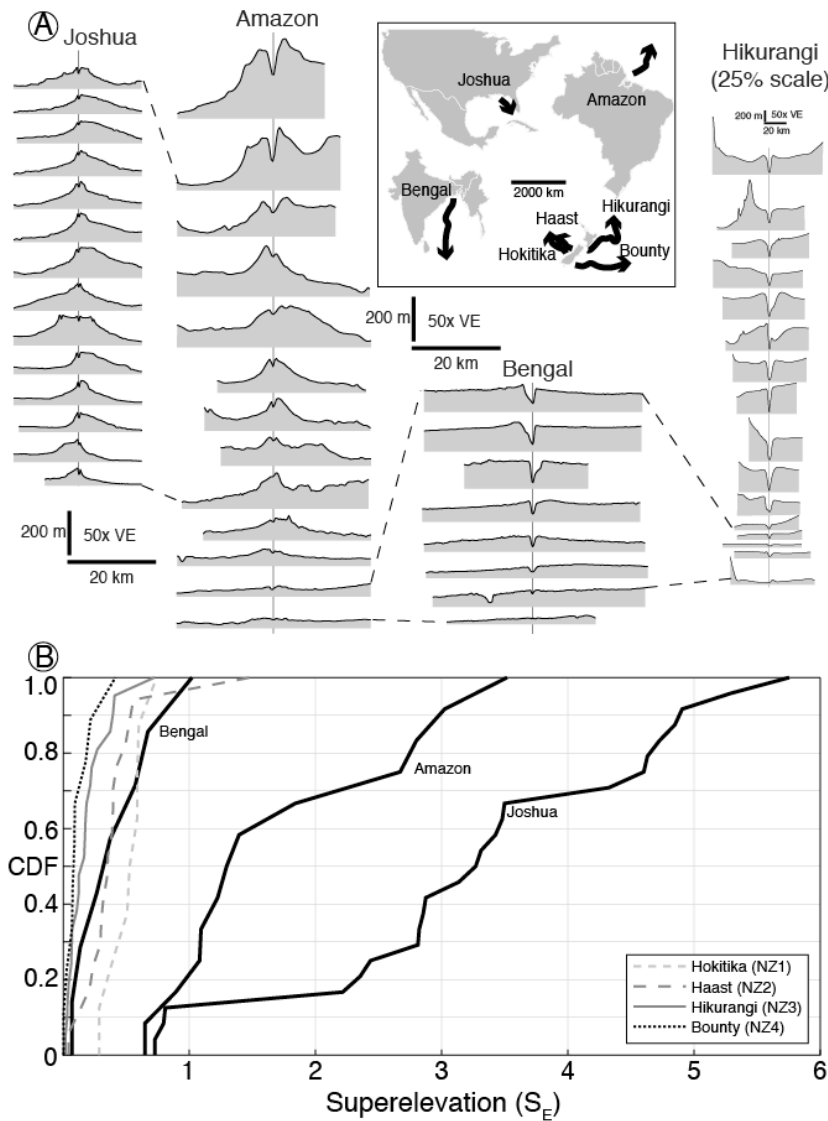
*Fig. 8. Submarine channels on the modern seafloor show variable superelevation. (A) Cross sections of modern submarine channels (inset map for location). Dashed lines indicate approximately equivalent streamwise portions of the four channel systems. (B) Calculated superelevation values indicate that passive-margin systems commonly attain higher superelevation, perhaps due to development of an equilibrium profile and strong channel-floodplain coupling. Note that the studied portion of the Bengal channel is quite distal (see part A), and thus not highly superelevated. The Hikurangi channel and other active-margin channels around New Zealand cannot build an equilibrium profile and thus display weak channel-floodplain coupling, with little levee development and thus low values of superelevation.*

## Downstream changes in channel-belt dimensions in the Amazon submarine fan

The Amazon system is a well-characterized locale for understanding submarine fan/channel dynamics (Damuth and Kumar, 1975; Flood and Damuth, 1987; Pirmez and Flood, 1995; Pirmez and Imran, 2003; Jegou et al., 2008; Manson, 2009). Channel avulsion and its effects on fan growth have been demonstrated in the Amazon system (Damuth et al., 1983; Damuth and Flood, 1983; Damuth et al., 1988; Flood et al., 1991; Pirmez and Flood, 1995; Piper and Normark, 2001; Manson, 2009; Maslin, 2009). Pirmez and Flood (1995) established a naming scheme for Quaternary channel avulsions on the Amazon Fan, and this study focuses on three of those named channels (Fig. 9): 'Brown' (oldest), '1E', and 'Amazon' (youngest, and the modern, most recently active channel). While older channels (e.g., 'Aqua', 'Orange') and other channels/avulsions have been documented during the studied time period (e.g., 1A, 1B, 1C, 1D, 1F; see Pirmez and Flood, 1995), suitable seismic-reflection profiles are absent or insufficient for full characterization. Fig. 9 shows a map of the Brown, 1E, and Amazon channels and their associated channel-belt cross sections. During Brown channel time, turbidity currents traversed through 16 cross sections from the canyon-channel transition to the last mapped Brown channel location (Fig. 9). An avulsion to the northwest created the 1E channel, which is constrained by 21 cross sections (Fig. 9). Finally, the most recent avulsion (again to the northwest) created the Amazon channel, which is constrained by 21 cross sections (Fig. 9). It is important to note that all turbidity currents that built the Brown, 1E, and Amazon channels traversed through the 14 most upstream cross sections, denoted as vertically stacked color gradients in  Fig. 9 and stacked datapoints in Fig. 10. We measured channel-belt dimensions at each cross-section location from the seafloor to the base of the oldest channel-belt genetically linked to that cross-section (Fig. 9; e.g., base-Brown for the 14 cross section furthest upstream, then base-1E for the next 4 cross-sections, etc.). This is the most accurate method available to measure true channel-belt dimensions, but it does not account for modification of the channel and channel-belt morphology that has likely occurred post-Brown and post-1E (i.e., during development of the modern Amazon channel. Fig. 9). Since there presently is no way to reconstruct the channel dimensions for Brown and 1E time at each cross-section location, we utilize modern seafloor channel and levee dimensions (e.g., $H$, $L_R$) to compare all three channel belts (Brown, 1E, Amazon).
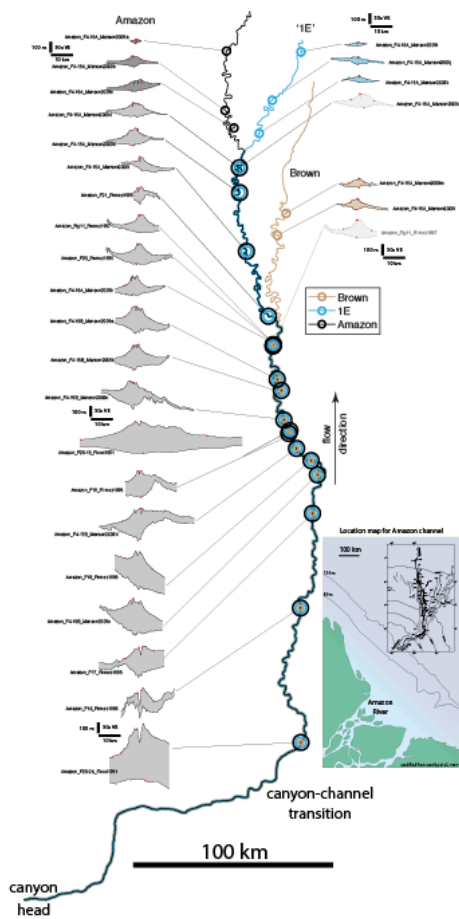
*Fig. 9. Amazon map showing location of the Brown, 1E, and modern Amazon channel segments, as well as the location of channel cross-sections derived from seismic reflection data. Inset shows the location of the Amazon fan-channel system offshore Brazil.*

Channel and channel-belt metrics generally show pronounced decreases downstream (Fig. 10). Channel cross-sectional area in all three channel-belts (Brown, 1E, and Amazon) decreases by nearly 100x downstream (Fig. 10A). We also computed the area of the channel belt (gray area between the points defining the floodplain, Fig. 3) as a proxy for total sediment volume contained within the channel belt (Fig. 4; Fig. 10B). The channel belt area also shows a steady downstream decrease in each of the three channel belts, with nearly two orders of magnitude of total change (Fig. 10B). Channel belt parameters that record aggradation ($H_{CB}$, $A_F$, $A_C$) show consistent decreasing values downstream (Fig. 10C, D, E), with total change from upstream to downstream approximately 10-fold. Levee relief ($L_R$) also decreases consistently downstream, with upstream values near 200 m and downstream values of only 10 m (Fig. 10F). This downstream decrease in $L_R$ is well documented for the Amazon system (e.g., Fig. 4 of Damuth and Flood, 1983; Piper and Normark, 2001; Pirmez and Imran, 2003) and other large, leveed submarine channel systems (e.g., Zaire system, Babonneau et al., 2002, 2010).

These downstream-thinning trends in channel-belt parameters are consistent with qualitative models of submarine fan growth (Mutti and Normark, 1987; Damuth et al., 1988). However, $S_E$ and $\chi$ show very different trends that are related to submarine channel avulsion dynamics. Upstream $S_E$ is relatively low ($S_E \sim 1$), but increases downstream to the Brown avulsion location, where $S_E$ values approach 6 (Fig. 10G). Downstream of the Brown avulsion, $S_E$ values for Brown significantly decrease, consistent with models of autogenic channel avulsion dynamics (Brizga and Finlayson, 1990; Mohrig et al., 2000). While we cannot rule out the possibility that $L_R$ and/or H were modified post-Brown and post-1E and these values of $S_E$ are not accurate, the close proximity of three independently-measured cross-sections have almost identical values of $S_E \sim 6$ (Fig. 10G; Fig. 9), suggesting this value may be the avulsion 'setup' for the modern Amazon channel. For the 1E channel, the avulsion location is not marked by a large $S_E$ value (Fig. 10G), suggesting that either (1) $L_R$ and H are not accurately measured or have been modified by the Amazon channel at this locale, or (2) that the 1E avulsion was caused by allogenic forcing (e.g., in-channel mass transport deposition, levee failure) rather than a large value of $S_E$. While poor absolute age control prevents us from unequivocally demonstrating an allogenic trigger at 1E time, Maslin (2009) reports emplacement of a large mass transport deposit at approximately 1E time, supporting one potential allogenic mechanism. If these trends in downstream $S_E$ are correct, the next autogenic avulsion in the Amazon system should occur near the Brown channel avulsion, as this remains the highest measured $S_E$ (Fig. 10G; Fig. 9). Why the channel has remained stable at this location with $S_E \sim 6$ is not clear but suggests that submarine channels are quite stable in highly aggradational settings (cf. Dorrell et al. 2015). Channel-floodplain coupling is strong and consistent in the Amazon system, with values of $\chi \sim 2$ for approximately 400 km (Fig. 10H). Interestingly, the Brown and 1E avulsions do not result in a change in $\chi$, indicating that strong channel-floodplain coupling is inherent to submarine channel systems. Modification of $\chi$ from a value of $\sim 2$ seems to be related to local factors; for example, very high values of $\chi$ exist in the canyon-channel transition zone, and the distalmost measurement has a very low $\chi$ value (Fig. 10H).

Using Equation 8, we would predict that with variable $S_E$ and consistent $\chi$, the normalized channel-belt thickness ($H_{CB}/H$) would mimic the trend of $S_E$. Indeed, our measurements of $H_{CB}/H$ show the highest values just upstream of the Brown avulsion location, supporting our theory of channel-belt aggradation and avulsion. The very large $H_{CB}/H$ measurement at $\sim 420$ km (cross section F23-13, Flood et al., 1991) may have been caused by the improper selection of channel-belt base, resulting in a channel belt that is falsely thick; however, this was chosen by Flood et al. (1991) and we have no data to provide an alternate interpretation.
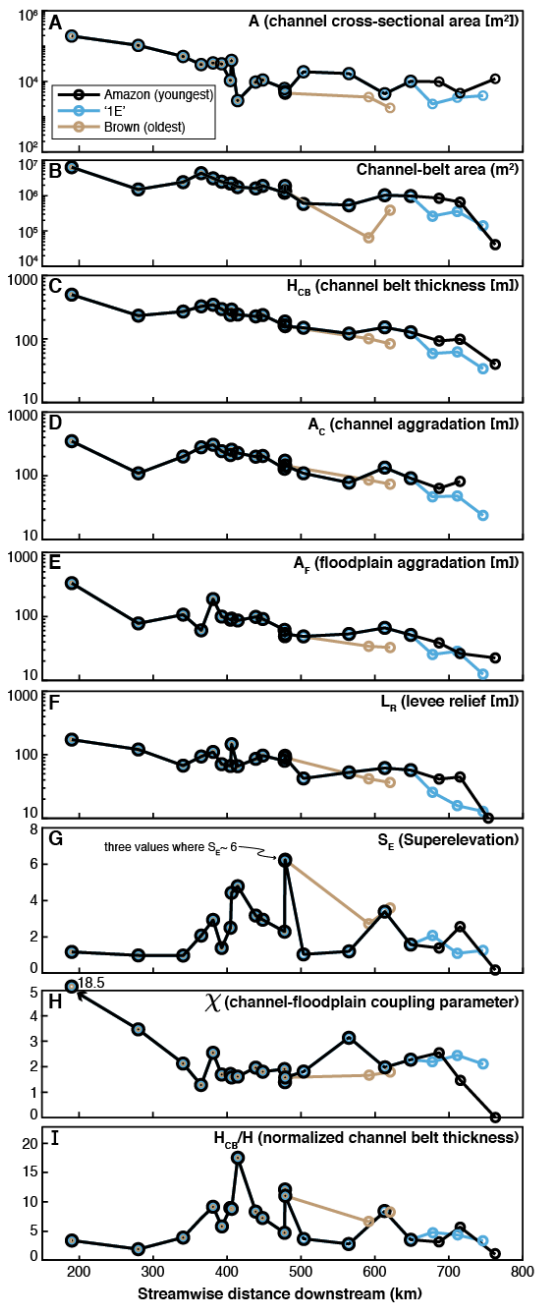
Fig. 10. Downstream channel-belt metrics for the Amazon submarine channel system. Most channel and channel-belt metrics show a distinct downstream decrease, consistent with models of channel-belt evolution and aggradation. However, superelevation (G) shows low values upstream (near the canyon-channel transition) and a peak near the Brown-channel avulsion node, indicating a potential linkage between superelevation and avulsion location. In (H), note the consistent values of $\chi$, indicating strong channel-floodplain coupling throughout the downstream channel evolution. Normalized channel-belt thickness (I) also shows this relationship, supporting the formulation of Equation 8.

# Conclusions

Avulsions are important drivers for creating channelized stratigraphy in both fluvial and submarine channel systems, and constraining the avulsion setup is critical for predicting the distribution of sediment, organic matter and pollutants. The aggradation of the channel, levee, and floodplain are the dominant drivers for avulsion dynamics, and they can be related in a geometric form. This study establishes a geometric channel-belt framework for predicting avulsions for both rivers and submarine channels and provides the first reported avulsion criteria for submarine channels. Prior studies have focused on superelevation of the channel above the floodplain, an important predictor of avulsion for rivers. While rivers can only superelevate an amount equivalent to 1 channel depth above the floodplain prior to avulsion, submarine channels are more stable during aggradation, and we document new data demonstrating superelevation values >3 channel depths.

This results in a normalized channel-belt thickness for submarine channels that can be as thick as ~ 10 channel depths, while fluvial channel belts are limited to a belt thickness of 2 channel depths. This disparity is caused by the differences in superelevation, but also by differences in channel-floodplain coupling. Since floodplain aggradation values in fluvial channel belts are only 1-10% compared to channel aggradation, it contributes a negligible amount to channel belt thickness and thus can be disregarded. In submarine channels, however, floodplain aggradation is important due to levee overspill and hemipelagic deposition and can be as large as 10-50% compared to channel aggradation. We summarize these observations with a coupling parameter chi ($\chi$) that relates floodplain to channel aggradation $A_C/(A_C-A_F)$. This coupling parameter is effectively 1 for rivers but ranges from 1 to 6 for submarine channels.

Submarine channels can be up to 10 times thicker than rivers at avulsion due to enhanced superelevation and channel-floodplain coupling, and we interpret that these enhancements are related to the unique flow properties of turbidity currents. Levee aggradation and thus superelevation is promoted by overspill (i.e., overbanking) from flows with 50x less density contrast as compared to rivers. Submarine floodplains are quite aggradational as well, contributing significantly to channel-belt growth. When the channel is perched far above the floodplain (i.e., significantly superelevated), there is far less potential energy in the flow as compared to a river, leading to a stable, aggradational channel. We demonstrate this stability using downstream trends in the Amazon channel, where superelevation and the

channel-floodplain coupling parameter $\chi$ remain at 2 or greater for more than 400 streamwise km, resulting in a channel belt that is ~ 5 channel-depths thick, more than twice the aggradation that a river is capable of.

# Acknowledgements

# References

Aalto, R., Lauer, J.W., and Dietrich, W.E., 2008, Spatial and temporal dynamics of sediment accumulation and exchange along Strickland River floodplains (Papua New Guinea) over decadal-to-centennial timescales: Journal of Geophysical Research: Earth Surface, v. 113, p. F01S04, doi:10.1029/2006JF000627.

Armitage, D.A., McHargue, T., Fildani, A., and Graham, S.A., 2012, Postavulsion channel evolution: Niger Delta continental slope: AAPG Bulletin, v. 96, 1p. 823–843, http://search.datapages.com/data/doi/10.1306/09131110189.

Azpiroz-Zabala, M., Cartigny, M.J.B., Talling, P.J., Parsons, D.R., Sumner, E.J., Clare, M.A., Simmons, S.M., Cooper, C., and Pope, E.L., 2017, Newly recognized turbidity current structure can explain prolonged flushing of submarine canyons: Science Advances, v. 3, p. e1700200, http://advances.sciencemag.org/lookup/doi/10.1126/sciadv.1700200.

Babonneau, N., Savoye, B., Cremer, M., and Bez, M., 2010, Sedimentary Architecture in Meanders of a Submarine Channel: Detailed Study of the Present Congo Turbidite Channel (Zaiango Project): Journal of Sedimentary Research, v. 80, p. 852–866, http://jsedres.sepmonline.org/cgi/doi/10.2110/jsr.2010.078.

Babonneau, N., Savoye, B., Cremer, M., and Klein, B., 2002, Morphology and architecture of the present canyon and channel system of the Zaire deep-sea fan: Marine and Petroleum Geology, v. 19, p. 445–467, http://www.sciencedirect.com/science/article/pii/S0264817202000090.

Berlin, T.L., 2014, Channel-Levee Complexes And Sediment Flux Of The Upper Indus Fan, Arabian Sea. Louisiana State University thesis, http://etd.lsu.edu/docs/available/etd-01172014-124019/.

Bonnel, C., Dennielou, B., Droz, L., Mulder, T., and Berné, S., 2005, Architecture and depositional pattern of the Rhône Neofan and recent gravity activity in the Gulf of Lions (western Mediterranean): Marine and Petroleum Geology, v. 22, p. 827–843, http://linkinghub.elsevier.com/retrieve/pii/S026481720500053X.

Bridge, J.S., and Leeder, M.R., 1979, A simulation model of alluvial stratigraphy: Sedimentology, v. 26, p. 617–644, https://onlinelibrary.wiley.com/doi/full/10.1111/j.1365-3091.1979.tb00935.x.

Brizga, S.O., and Finlayson, B.L., 1990, Channel avulsion and river metamorphosis: The case of the Thomson River, Victoria, Australia: Earth Surface Processes and Landforms, v. 15, p. 391–404, https://onlinelibrary.wiley.com/doi/full/10.1002/esp.3290150503.

Bryant, M., Falk, P., and Paola, C., 1995, Experimental study of avulsion frequency and rate of deposition: Geology, v. 23, p. 365–368, https://pubs.geoscienceworld.org/geology/article/23/4/365-368/206294.

Buffington, E.C., 1952, Submarine" Natural Levees": The Journal of Geology, http://www.jstor.org/stable/30058339.

Damuth, J.E., Flood, R.D., and Kowsmann, R.O., 1988, Anatomy and growth pattern of Amazon deep-sea fan as revealed by long-range side-scan sonar (GLORIA) and high-resolution seismic studies: AAPG Bulletin, http://archives.datapages.com/data/bulletns/1988-89/data/pg/0072/0008/0850/0885.htm.

Damuth, J.E., and Kumar, N., 1975, Amazon Cone: morphology, sediments, age, and growth pattern: Geological Society of America Bulletin, v. 86, p. 863-878, http://gsabulletin.gsapubs.org/content/86/6/863.short.

Damuth, J.E., and Flood, R.D., 1983, Morphology, sedimentation processes, and growth pattern of the Amazon Deep-Sea Fan: Geo-Marine Letters, v. 3, p. 109–117, https://link.springer.com/article/10.1007/BF02462455.

Damuth, J.E., Kowsmann, R.O., Flood, R.D., Belderson, R.H., and Gorini, M.A., 1983, Age relationships of distributary channels on Amazon deep-sea fan: Implications for fan growth pattern: Geology, v. 11, p. 470–473, https://pubs.geoscienceworld.org/geology/article/11/8/470-473/203557.

Dietrich, W.E., and Whiting, P., 1989, Boundary shear stress and sediment transport in river meanders of sand and gravel, p. 1–50, in Ikeda, S., and Parker, G., River Meandering 12, doi:10.1029/WM012p0001.

Dorrell, R.M., Darby, S.E., Peakall, J., Sumner, E.J., Parsons, D.R., and Wynn, R.B., 2014, The critical role of stratification in submarine channels: Implications for channelization and long runout of flows: Journal of Geophysical Research: Oceans, v. 119, p. 2620–2641, http://doi.wiley.com/10.1002/2014JC009807.

Dorrell, R.M., Burns, A.D., and McCaffrey, W.D., 2015, The inherent instability of leveed seafloor channels: Geophysical Research Letters, v. 42, p. 4023–4031, http://doi.wiley.com/10.1002/2015GL063809.

Droz, L., Marsset, T., Ondras, H., and Lopez, M., 2003, Architecture of an active mud-rich turbidite system: The Zaire Fan (Congo–Angola margin southeast Atlantic): Results from ZaAngo 1 and 2 cruises: AAPG Bulletin, v. 87, p. 1145–1168, http://archives.datapages.com/data/doi/10.1306/03070300013.

Edmonds, D.A., Hoyal, D.C.J.D., Sheets, B.A., and Slingerland, R.L., 2009, Predicting delta avulsions: Implications for coastal wetland restoration: Geology, v. 37, p. 759–762, doi:10.1130/G25743A.1.

Ferguson, R.J., and Brierley, G.J., 1999, Levee morphology and sedimentology along the lower Tuross River, south-eastern Australia: Sedimentology, v. 46, p. 627–648, https://onlinelibrary.wiley.com/doi/full/10.1046/j.1365-3091.1999.00235.x.

Fernandes, A.M., Törnqvist, T.E., Straub, K.M., and Mohrig, D., 2016, Connecting the backwater hydraulics of coastal rivers to fluvio-deltaic sedimentology and stratigraphy: Geology, v. 44, p. 979–982, http://geology.gsapubs.org/lookup/doi/10.1130/G37965.1.

Fildani, A., Normark, W.R., Kostic, S., and Parker, G., 2006, Channel formation by flow stripping: large-scale scour features along the Monterey East Channel and their relation to sediment waves: Sedimentology, v. 53, p. 1265–1287, http://doi.wiley.com/10.1111/j.1365-3091.2006.00812.x.

Flood, R. D., C. Pirmez, and H. Yin., 1997, The compressional-wave velocity of Amazon Fan sediments: Calculation from index properties and variation with clay content. Proceedings of the Ocean Drilling Program. Scientific results. Vol. 155. Ocean Drilling Program.

Flood, R.D., and Damuth, J.E., 1987, Quantitative characteristics of sinuous distributary channels on the Amazon Deep-Sea Fan: Geological Society of America Bulletin, v. 98, p. 728–738, http://gsabulletin.gsapubs.org/cgi/doi/10.1130/0016-7606(1987)98%3C728:QCOSDC%3E2.0.CO.

Flood, R.D., Manley, P.L., Kowsmann, R.O., Appi, C.J., and Pirmez, C., 1991, Seismic Facies and Late Quaternary Growth of Amazon Submarine Fan BT - Seismic Facies and Sedimentary Processes of Submarine Fans and Turbidite Systems, in Seismic Facies and Sedimentary Processes of Submarine Fans and Turbidite Systems, New York, NY, Springer New York, p. 415–433, http://link.springer.com/10.1007/978-1-4684-8276-8_23.

Ganti, V., Chadwick, A.J., Hassenruck-Gudipati, H.J., and Lamb, M.P., 2016, Avulsion cycles and their stratigraphic signature on an experimental backwater-controlled delta: Journal of Geophysical Research: Earth Surface, v. 121, p. 1651–1675, doi:10.1002/2016JF003915.

Hajek, E.A., and Edmonds, D.A., 2014, Is river avulsion style controlled by floodplain morphodynamics? Geology, v. 42, p. 199–202, doi:10.1130/G35045.1.

Hansen, L., Callow, R., Kane, I., and Kneller, B., 2017, Differentiating submarine channel-related thin-bedded turbidite facies: Outcrop examples from the Rosario Formation, Mexico: Sedimentary Geology, v. 358, p. 19–34, http://dx.doi.org/10.1016/j.sedgeo.2017.06.009.

Hay, A.E., 1987, Turbidity currents and submarine channel formation in Rupert Inlet, British Columbia: 2. The roles of continuous and surge-type flow: Journal of Geophysical Research, v. 92, p. 2883–2900, http://onlinelibrary.wiley.com/doi/10.1029/JC092iC03p02883/full.

Heller, P.L., and Paola, C., 1996, Downstream changes in alluvial architecture; an exploration of controls on channel-stacking patterns: Journal of Sedimentary Research, v. 66, p. 297–306, http://archives.datapages.com/data/doi/10.1306/D4268333-2B26-11D7-8648000102C1865D.

Hiscott, R. N., Hall, F. R., & Pirmez, C., 1997, Turbidity-current overspill from the Amazon Channel: texture of the silt/sand load, paleoflow from anisotropy of magnetic susceptibility, and implications for flow processes. Proceedings of the Ocean Drilling Program. Scientific results, vol. 155, Ocean Drilling Program.

Hübscher, C., Spieβ, V., Breitzke, M., and Weber, M.E., 1997, The youngest channel-levee system of the Bengal Fan: Results from digital sediment echosounder data: Marine Geology, v. 141, p. 125–145, http://linkinghub.elsevier.com/retrieve/pii/S0025322797000662.

Imran, J., Parker, G., and Katopodes, N., 1998, A numerical model of channel inception on submarine fans: Journal of Geophysical Research, v. 103, p. 1219–1238, http://onlinelibrary.wiley.com/doi/10.1029/97JC01721/full.

Imran, J., Parker, G., and Pirmez, C., 1999, A nonlinear model of flow in meandering submarine and subaerial channels: Journal of Fluid Mechanics, v. 400, p. 295–331, http://journals.cambridge.org/action/displayAbstract?aid=15539.

Jegou, I., Savoye, B., Pirmez, C., and Droz, L., 2008, Channel-mouth lobe complex of the recent Amazon Fan: The missing piece: Marine Geology, v. 252, p. 62–77, http://linkinghub.elsevier.com/retrieve/pii/S0025322708000777.

Jerolmack, D.J., 2009, Conceptual framework for assessing the response of delta channel networks to Holocene sea level rise: Quaternary Science Reviews, v. 28, p. 1786–1800, http://dx.doi.org/10.1016/j.quascirev.2009.02.015.

Jerolmack, D.J., and Mohrig, D., 2007, Conditions for branching in depositional rivers: Geology, v. 35, p. 463–466, http://geology.gsapubs.org/cgi/doi/10.1130/G23308A.1.

Jobe, Z.R., Lowe, D.R., and Uchytil, S.J., 2011, Two fundamentally different types of submarine canyons along the continental margin of Equatorial Guinea: Marine and Petroleum Geology, v. 28, p. 843–860, http://dx.doi.org/10.1016/j.marpetgeo.2010.07.012.

Jobe, Z.R., Howes, N.C., and Auchter, N.C., 2016, Comparing submarine and fluvial channel kinematics: Implications for stratigraphic architecture: Geology, v. 44, p. 931–934, doi:10.1130/G38158.1.

Jobe, Z.R., Sylvester, Z., Pittaluga, M.B., Frascati, A., Pirmez, C., Minisini, D., Howes, N.C., and Cantelli, A., 2017, Facies architecture of submarine channel deposits on the western Niger Delta slope: Implications for grain-size and density stratification in turbidity currents: Journal of Geophysical Research: Earth Surface, v. 122, p. 473–491, http://doi.wiley.com/10.1002/2016JF003903.

Johnston, G.H., David, S.R., and Edmonds, D.A., 2019, Connecting Fluvial Levee Deposition to Flood-Basin Hydrology: Journal of Geophysical Research: Earth Surface, doi:10.1029/2019jf005014.

Jones, L.S., and Schumm, S.A., 1999, Causes of Avulsion: An Overview, in Fluvial Sedimentology VI, Vol. 28, pp. 171-178 Oxford, UK, Blackwell Publishing Ltd., doi:10.1002/9781444304213.ch13.

Kenyon, N.H., Amir, A., And Cramp, A., 1995, Geometry of the younger sediment bodies of the Indus Fan, in Pickering, K.T., Hiscott, R.N., Kenyon, N.H., Ricci Lucchi, F., and Smith R.D.A., eds., Atlas of Deep Water Environments; Architectural Style in Turbidite Systems, Oxford, U.K., Chapman & Hall, p. 89–93.

Kolla, V., 2007, A review of sinuous channel avulsion patterns in some major deep-sea fans and factors controlling them: Marine and Petroleum Geology, v. 24, p. 450–469, http://linkinghub.elsevier.com/retrieve/pii/S0264817207000359.

Kolla, V., Bandyopadhyay, A., Gupta, P., Mukherjee, B., and Ramana, D.V., 2012, Morphology and internal structure of a recent upper Bengal fan valley complex, in Prather, B.E., et al., eds., Application of the principles of seismic geomorphology to continental-slope and base-of-slope systems: Case studies from seafloor and near-seafloor analogues: SEPM (Society for Sedimentary Geology) Special Publication 99, p. 347–369, doi:10.2110/pec.12.99.0347.

Kolla, V., Posamentier, H.W., and Wood, L.J., 2007, Deep-water and fluvial sinuous channels—Characteristics, similarities and dissimilarities, and modes of formation: Marine and Petroleum Geology, v. 24, p. 388–405, http://linkinghub.elsevier.com/retrieve/pii/S0264817207000281.

Konsoer, K., Zinger, J., and Parker, G., 2013, Bankfull hydraulic geometry of submarine channels created by turbidity currents: Relations between bankfull channel characteristics and formative flow discharge: Journal of Geophysical Research: Earth Surface, v. 118, p. 216–228, http://doi.wiley.com/10.1029/2012JF002422.

Leeder, M.R., 1978, A quantitative stratigraphic model for alluvium, with special reference to channel deposit density and interconnectedness, in eds. Miall, A., Fluvial Sedimentology, Mem. Can. Soc. Pet. Geol., vol. 5, p. 587-596, http://archives.datapages.com/data/dgs/005/005001/587_cspgsp0050587.htm.

Leslie, S., Cordon, I., and Lopez-Gamundi, O., 2012, Pleistocene to Recent Channel / Levee System from the Slope of the Magdalena Fan:, http://www.earthdoc.org/publication/publicationdetails/?publication=66227.

Lewin, J., and Ashworth, P.J., 2014, The negative relief of large river floodplains: Earth Science Reviews, v. 129, p. 1–23, http://dx.doi.org/10.1016/j.earscirev.2013.10.014.

Lopez, M., 2001, Architecture and depositional pattern of the Quaternary deep-sea fan of the Amazon: Marine and Petroleum Geology, v. 18, p. 479–486, http://linkinghub.elsevier.com/retrieve/pii/S0264817200000714.

Makaske, B., Smith, D.G., and Berendsen, H.J.A., 2002, Avulsions, channel evolution and floodplain sedimentation rates of the anastomosing upper Columbia River, British Columbia, Canada: Sedimentology, v. 49, p. 1049–1071, doi:10.1046/j.1365-3091.2002.00489.x.

Manson, S., 2009, Avulsion process : stratigraphic and lithologic records - Application to the Amazon and Zaire turbidite systems: Université de Bretagne occidentale - Brest, https://tel.archives-ouvertes.fr/tel-00940151/document.

Marsset, T., Droz, L., Dennielou, B., & Pichon, E., 2009, Cycles in the architecture of the Quaternary Zaire turbidite system: a possible link with climate. External Controls on Deep-Water Depositional Systems. SEPM Special Publication 92, 89-106.

Martin, J., Fernandes, A.M., Pickering, J., Howes, N., Mann, S., and McNeil, K., 2018, The Stratigraphically Preserved Signature of Persistent Backwater Dynamics in a Large Paleodelta System: The Mungaroo Formation, North West Shelf, Australia: Journal of Sedimentary Research, v. 88, p. 850–872, doi:10.2110/jsr.2018.38.

Maslin, M. A., 2009, Review of the timing and causes of the Amazon-Fan mass transport and avulsion deposits during the latest Pleistocene. External controls on deep-water depositional systems, SEPM Special Publication 92, 133-144.

Mikkelsen, N., Maslin, M., Giraudeau, J., and Showers, W., 1997, 38. Biostratigraphy And Sedimentation Rates Of The Amazon Fan, Proceedings of the Ocean Drilling Program. Scientific results, vol. 155, Ocean Drilling Program.

Mohrig, D., Heller, P.L., and Paola, C., 2000, Interpreting avulsion process from ancient alluvial sequences: Guadalope-Matarranya system (northern Spain) and Wasatch Formation (western Colorado): Geological Society of America Bulletin, v. 112, p. 1787–1803, http://gsabulletin.gsapubs.org/content/112/12/1787.short.

Mountjoy, J.J., Barnes, P.M., and Pettinga, J.R., 2009, Morphostructure and evolution of submarine canyons across an active margin: Cook Strait sector of the Hikurangi Margin, New Zealand: Marine Geology, v. 260, p. 45–68, http://dx.doi.org/10.1016/j.margeo.2009.01.006.

Mutti, E., & Normark, W. R., 1987, Comparing examples of modern and ancient turbidite systems: problems and concepts. In Marine clastic sedimentology (pp. 1-38). Springer, Dordrecht.

Nakajima, T., Satoh, M., and Okamura, Y., 1998, Channel-levee complexes, terminal deep-sea fan and sediment wave fields associated with the Toyama Deep-Sea Channel system in the Japan Sea: Marine Geology, v. 147, p. 25–41, http://linkinghub.elsevier.com/retrieve/pii/S0025322797001370.

Nakajima, T., and Kneller, B.C., 2012, Quantitative analysis of the geometry of submarine external levées. Sedimentology, v. 60, p. 877–910, http://doi.wiley.com/10.1111/j.1365-3091.2012.01366.x.

Nittrouer, J.A., Shaw, J., Lamb, M.P., and Mohrig, D., 2012, Spatial and temporal trends for water-flow velocity and bed-material sediment transport in the lower Mississippi River: Geological Society of America Bulletin, v. 124, p. 400–414, http://gsabulletin.gsapubs.org/cgi/doi/10.1130/B30497.1.

Nittrouer, J.A., Mohrig, D., Allison, M.A., And Peyret, A.-P.B., 2011, The lowermost Mississippi River: a mixed bedrock-alluvial channel: Sedimentology, v. 58, p. 1914–1934, http://doi.wiley.com/10.1111/j.1365-3091.2011.01245.x.

Normark, W.R., and Damuth, J.E., 1997, Sedimentary facies and associated depositional elements of the Amazon Fan. Proceedings of the Ocean Drilling Program. Scientific results, vol. 155, Ocean Drilling Program.

Normark, W.R., Posamentier, H., and Mutti, E., 1993, Turbidite systems: State of the art and future directions: Reviews of Geophysics, v. 31, p. 91−116, doi:10.1029/93RG02832.

Ortiz-Karpf, A., Hodgson, D.M., and McCaffrey, W.D., 2015, The role of mass-transport complexes in controlling channel avulsion and the subsequent sediment dispersal patterns on an active margin: The Magdalena Fan, offshore Colombia: Marine and Petroleum Geology, v. 64, p. 58−75, http://dx.doi.org/10.1016/j.marpetgeo.2015.01.005.

Peakall, J., McCaffrey, B., and Kneller, B., 2000, A Process Model for the Evolution, Morphology, and Architecture of Sinuous Submarine Channels: Journal of Sedimentary Research, v. 70, p. 434–448, http://jsedres.sepmonline.org/content/70/3/434.full.

Picot, M., Droz, L., Marsset, T., Dennielou, B., and Bez, M., 2016, Controls on turbidite sedimentation: Insights from a quantitative approach of submarine channel and lobe architecture (Late Quaternary Congo Fan): Marine and Petroleum Geology, v. 72, p. 423–446, http://dx.doi.org/10.1016/j.marpetgeo.2016.02.004.

Piper, D.J.W., and Deptuck, M., 1997, Fine-grained turbidites of the Amazon Fan: facies characterization and interpretation. Proceedings of the Ocean Drilling Program. Scientific results, vol. 155, Ocean Drilling Program.

Piper, D.J.W., and Normark, W.R., 1983, Turbidite Depositional Patterns and Flow Characteristics, Navy Submarine Fan, California Borderland: Sedimentology, v. 30, p. 681–694, http://doi.wiley.com/10.1111/j.1365-3091.1983.tb00702.x.

Piper, D.J.W., and Normark, W.R., 2001, Sandy fans--from Amazon to Hueneme and beyond: AAPG Bulletin, v. 85, p. 1407−1438, http://archives.datapages.com/data/bulletns/2001/08aug/1407/1407.htm.

Pirmez, C., and Flood, R.D., 1995, Morphology and Structure of Amazon Channel. Proceedings of the Ocean Drilling Program. Initial Reports, vol. 155, Ocean Drilling Program.

Pirmez, C., Hiscott, R.N., and Kronen, J., 1997, Sandy turbidite successions at the base of channel-levee systems on the Amazon Fan: unraveling the facies architecture of large submarine fans. Proceedings of the Ocean Drilling Program. Scientific results, vol. 155, Ocean Drilling Program.

Pirmez, C., and Imran, J., 2003, Reconstruction of turbidity currents in Amazon Channel: Marine and Petroleum Geology, v. 20, p. 823−849, http://linkinghub.elsevier.com/retrieve/pii/S0264817203001302.

Pizzuto, J.E., 1987, Sediment Diffusion During Overbank Flows: Sedimentology, v. 34, p. 301−317.

Popescu, I., Lericolais, G., Panin, N., Wong, H.K., and Droz, L., 2001, Late Quaternary channel avulsions on the Danube deep-sea fan, Black Sea: Marine Geology, v. 179, p. 25−37, http://linkinghub.elsevier.com/retrieve/pii/S0025322701001979.

Posamentier, H.W., 2003, Depositional elements associated with a basin floor channel-levee system: case study from the Gulf of Mexico: Marine and Petroleum Geology, v. 20, p. 677−690, http://linkinghub.elsevier.com/retrieve/pii/S0264817203001247.

Schwenk, T., and Spieß, V., 2009, Architecture and stratigraphy of the Bengal Fan as response to tectonic and climate revealed from high-resolution seismic data. External controls on deep-water depositional systems, SEPM Special Publication 92, 133-144.

Schwenk, T., Spiess, V., Hübscher, C., and Breitzke, M., 2003, Frequent channel avulsions within the active channel–levee system of the middle Bengal Fan—an exceptional channel–levee development derived from Parasound and Hydrosweep data: Deep Sea Research Part II: Topical Studies in Oceanography, v. 50, p. 1023−1045, http://linkinghub.elsevier.com/retrieve/pii/S0967064502006185.

Sequeiros, O.E., Spinewine, B., and Beaubouef, R.T., 2010, Characteristics of velocity and excess density profiles of saline underflows and turbidity currents flowing over a mobile bed: Journal of Hydraulic Engineering, v. 10.1061/(A, p. 412−433, http://ascelibrary.org/doi/abs/10.1061/(ASCE)HY.1943-7900.0000200.

Shen, Z., Törnqvist, T.E., Mauz, B., Chamberlain, E.L., Nijhuis, A.G., and Sandoval, L., 2015, Episodic overbank deposition as a dominant mechanism of floodplain and delta-plain aggradation: Geology, v. 43, p. 875−878, doi:10.1130/G36847.1.

Shumaker, L.E., Jobe, Z.R., Johnstone, S.A., Pettinga, L.A., Cai, D., and Moody, J.D., 2018, Controls on submarine channel-modifying processes identified through morphometric scaling relationships: Geosphere, v. 14, p. 1−17, doi:10.1130/GES01674.1.

Shumaker, L.E., Jobe, Z.R., and Graham, S.A., 2017, Evolution of submarine gullies on a prograding slope: Insights from 3D seismic reflection data: Marine Geology, v. 393, p. 35–46, doi:10.1016/j.margeo.2016.06.006.

Skene, K.I., Piper, D.J.W., and Hill, P.S., 2002, Quantitative analysis of variations in depositional sequence thickness from submarine channel levees: Sedimentology, v. 49, p. 1411–1430, http://onlinelibrary.wiley.com/doi/10.1046/j.1365-3091.2002.00506.x/full.

Slingerland, R., and Smith, N.D., 1998, Necessary conditions for a meandering-river avulsion: Geology, v. 26, p. 435–438, http://gateway.webofknowledge.com/gateway/Gateway.cgi?GWVersion=2&SrcAuth=mekentosj&SrcApp=Papers&DestLinkType=FullRecord&DestApp=WOS&KeyUT=000073509400013.

Slingerland, R., and Smith, N.D., 2004, River Avulsions And Their Deposits: Annual Review of Earth and Planetary Sciences, v. 32, p. 257–285, http://www.annualreviews.org/doi/10.1146/annurev.earth.32.101802.120201.

Smith, N.D., Cross, T.A., Dufficy, J.P., And Clough, S.R., 1989, Anatomy of an avulsion: Sedimentology, v. 36, p. 1–23, doi:10.1111/j.1365-3091.1989.tb00817.x.

Stelting, C.E., Droz, L.I., Bouma, A.H., Coleman, J.M., Cremer, M., Meyer, A.W., Normark, W.R., O'comsat, S., And Stow, D.A.V., 1986, Late Pleistocene seismic stratigraphy of the Mississippi Fan, in Bouma, A.H., Coleman, J.M., Brooks, J.M., et al., eds., Initial reports of the Deep Sea Drilling Project, v. 96, p. 437-456.

Stow, D.A. V, Huc, A.Y., and Bertrand, P., 2001, Depositional processes of black shales in deep water: Marine and Petroleum Geology, v. 18, p. 491–498, http://linkinghub.elsevier.com/retrieve/pii/S0264817201000125.

Stow, D.A. V, and Piper, D.J.W., 1984, Deep-water fine-grained sediments: facies models: Geological Society, London, Special Publications, v. 15, p. 611–646, http://sp.lyellcollection.org/cgi/doi/10.1144/GSL.SP.1984.015.01.38.

Straub, K.M., and Mohrig, D., 2008, Quantifying the morphology and growth of levees in aggrading submarine channels: Journal of Geophysical Research, v. 113, p. F03012, http://doi.wiley.com/10.1029/2007JF000896.

Strong, N., and Paola, C., 2008, Valleys That Never Were: Time Surfaces Versus Stratigraphic Surfaces: Journal of Sedimentary Research, v. 78, p. 579–593, http://jsedres.sepmonline.org/cgi/doi/10.2110/jsr.2008.059.

Sylvester, Z., Pirmez, C., and Cantelli, A., 2011, A model of submarine channel-levee evolution based on channel trajectories: Implications for stratigraphic architecture: Marine and Petroleum Geology, v. 28, p. 716–727, http://dx.doi.org/10.1016/j.marpetgeo.2010.05.012.

Torbjörn E. Törnqvist, 1994, Middle and late Holocene avulsion history of the River Rhine (Rhine-Meuse delta, Netherlands): Geology, v. 22, p. 771–714, doi:https://doi.org/10.1130/0091-7613(1994)022<0711:MALHAH>2.3.CO;2.

Törnqvist, T.E., and Bridge, J.S., 2002, Spatial variation of overbank aggradation rate and its influence on avulsion frequency: Sedimentology, v. 49, p. 891–905, doi:10.1046/j.1365-3091.2002.00478.x.

Torres, J., Droz, L., Savoye, B., Terentieva, E., Cochonat, P., Kenyon, N.H., and Canals, M., 1997, Deep-sea avulsion and morphosedimentary evolution of the Rhône Fan Valley and Neofan during the Late Quaternary (north-western Mediterranean Sea): Sedimentology, v. 44, p. 457–477, http://doi.wiley.com/10.1046/j.1365-3091.1997.d01-36.x.

Weber, M.E., Wiedicke, M.H., Kudrass, H.R., Hübscher, C., and Erlenkeuser, H., 1997, Active growth of the Bengal Fan during sea-level rise and highstand: Geology, v. 25, p. 315–318, http://geology.gsapubs.org/cgi/doi/10.1130/0091-7613(1997)025%3C0315:AGOTBF%3E2.3.CO.

Wolman, M.G. & Leopold, L.B., 1957, River flood plains: some observations on their formation. U.S. Geol. Surv. Prof. Paper, 282-C, 109 p.